

An interpretable neural network-based non-proportional odds model for ordinal regression with continuous response

Akifumi Okuno^{1,2} and Kazuharu Harada^{3,1}

¹The Institute of Statistical Mathematics

²RIKEN Center for Advanced Intelligence Project

³Tokyo Medical University

okuno@ism.ac.jp, haradak@tokyo-med.ac.jp

Abstract

This paper proposes an interpretable neural network-based non-proportional odds model (N³POM) for ordinal regression, where the response variable can take not only discrete but also continuous values, and the regression coefficients vary depending on the predicting ordinal response. In contrast to conventional approaches estimating the linear coefficients of regression directly from the discrete response, we train a non-linear neural network that outputs the linear coefficients by taking the response as its input. By virtue of the neural network, N³POM may have flexibility while preserving the interpretability of the conventional ordinal regression. We show a sufficient condition so that the predicted conditional cumulative probability (CCP) satisfies the monotonicity constraint locally over a user-specified region in the covariate space; we also provide a monotonicity-preserving stochastic (MPS) algorithm for training the neural network adequately.

Keywords: Continuous ordinal regression, Non-proportional odds model, Neural network

1 Introduction

Ordinal regression modeling treats the response as an ordinal scale and aims to understand the relationship between the order of the response and the covariates (Agresti, 2010). In the context of ordinal regression modeling, response variables are typically assumed to be ordinal and discrete (e.g., stage of cancer, scores of wine quality). While standard regression approaches are mainly interested in the actual value of the response, this paper focuses on thresholds of the responses, i.e., the probability of the response being less than or equal to a specific threshold as a function of the covariates.

Let $d, J \in \mathbb{N}$ and consider (G, X) , a pair of such a discrete ordinal response variable $G \in \{1, 2, \dots, J\}$ and its covariate $X \in \mathbb{R}^d$. A standard model for analyzing such a threshold is the proportional odds model (POM):

$$\mathbb{P}_{\text{POM}}(G \leq j \mid X = \mathbf{x}) = \sigma(\alpha_j + \langle \boldsymbol{\beta}, \mathbf{x} \rangle) \quad (j \in \{1, 2, \dots, J-1\}),$$

where $\sigma(z) = 1/(1 + \exp(z))$ is a sigmoid function, and $\alpha_1, \alpha_2, \dots, \alpha_{J-1} \in \mathbb{R}, \boldsymbol{\beta} \in \mathbb{R}^d$ are parameters to be estimated. This model satisfies the parallelism assumption (McCullagh, 1980), which states that the regression coefficients are equal across all thresholds. However, the parallelism assumption is often considered to be violated (see, e.g., Long and Freese (2006)). For example, in restaurant ratings, basic factors such as good hygiene would be considered important in lower scores, while factors like ingredient origin and wine selection would be seen more significant in higher scores. Also see Williams (2016) for discussion on the violation of the parallelism assumption, in the real-world situation.

One approach to circumvent the assumption violation is leveraging the non-proportional odds model (NPOM, a.k.a., generalized ordinal logit model):

$$\mathbb{P}_{\text{NPOM}}(G \leq j \mid X = \mathbf{x}) = \sigma(\alpha_j + \langle \boldsymbol{\beta}_j, \mathbf{x} \rangle) \quad (j \in \{1, 2, \dots, J-1\}),$$

that allows the coefficients to vary across the thresholds of the response. See, e.g., [McCullagh and Nelder \(1989\)](#), [Peterson and Harrell \(1990\)](#), and [Williams \(2006\)](#). However, there still remain several difficulties in leveraging NPOM.

- (D-1) The first difficulty is the lack of monotonicity of the predicted conditional cumulative probability (CCP), i.e., the predicted CCP may violate a monotonicity as $\hat{\mathbb{P}}_{\text{NPOM}}(G \leq j \mid X = \mathbf{x}) > \hat{\mathbb{P}}_{\text{NPOM}}(G \leq j+1 \mid X = \mathbf{x})$ for some (j, \mathbf{x}) , due to the flexibility of the varying coefficients ([Tutz and Berger, 2022](#); [Lu et al., 2022](#)). As the simple POM with $\alpha_1 \leq \alpha_2 \leq \dots \leq \alpha_J$ is obviously monotone in terms of the CCP, [Lu et al. \(2022\)](#) considers $\boldsymbol{\beta}_j = \boldsymbol{\beta}_* + \boldsymbol{\delta}_j$ with a prototype $\boldsymbol{\beta}_*$ and incorporates L^2 penalty to the deviation $\boldsymbol{\delta}_j$. [Tutz and Berger \(2022\)](#) further restricts the deviation as $\boldsymbol{\delta}_j = (j - J/2)\tilde{\boldsymbol{\delta}}$. [Wurm et al. \(2021\)](#) (a.k.a. ordinalNet) specifies the prototype as $\boldsymbol{\beta}_* = \mathbf{0}$ and incorporates elastic penalty, i.e., the sum of L^2 and L^1 penalties. They assert that a monotone CCP is obtained by increasing the penalty weights, as the NPOM then gets closer to the simple POM estimating only the prototype. However, the larger penalty weights may yield a larger bias, while smaller weights do not guarantee monotonicity; specifying the proper penalty weights still remains a problem.
- (D-2) The second difficulty is the lack of the proximity guarantee of the estimated coefficients for adjacent thresholds. As it is more natural if the adjacent coefficients are proximate, [Tutz and Gertheiss \(2016\)](#) and [Ugba et al. \(2021\)](#) incorporate a penalty between the coefficients of adjacent thresholds $\|\boldsymbol{\beta}_{j+1} - \boldsymbol{\beta}_j\|_2^2$. However, the adjacent penalty cannot be simply incorporated into the above monotonicity-guaranteed NPOM, due to the incompatibility with the optimization algorithm.
- (D-3) The third difficulty is the lack of extensibility to continuous responses; in some cases, we are interested in the probability that a continuous variable (e.g., item prices, lifetime of people) is less than or equal to a threshold. Existing methods training NPOM, that directly estimate countably many coefficients $\boldsymbol{\beta}_1, \boldsymbol{\beta}_2, \dots, \boldsymbol{\beta}_J$, cannot be simply extended to continuous response, as such a naive extension needs to estimate uncountably many coefficients $\{\boldsymbol{\beta}_u\}_{1 \leq u \leq J}$. As a study in the field of survival analysis, [Satoh et al. \(2016\)](#) relaxes the parallelism assumption in the continuous POM ([Bennett, 1983](#); [Kalbfleisch and Prentice, 2002](#)). However, no monotonicity guarantee is provided therein. Also see Section 2.3 for details.

As a first study that addresses all of these three difficulties simultaneously, we propose a *neural network-based NPOM* (N³POM):

$$\mathbb{P}_{\text{N}^3\text{POM}}(H \leq u \mid X = \mathbf{x}) = \sigma(a(u) + \langle \mathbf{b}(u), \mathbf{x} \rangle) \quad (u \in [1, J]),$$

where $H \in [1, J]$ is a continuous response variable associated with the covariate $X \in \mathbb{R}^d$ and $a : [1, J] \rightarrow \mathbb{R}$ is a piece-wise linear continuous function. We employ a non-linear neural network for the coefficient $\mathbf{b} : [1, J] \rightarrow \mathbb{R}^d$, so the continuity is naturally introduced to the varying coefficients. As we train the neural network for estimating the coefficients of the linear model instead of modeling the cumulative probability directly, the proposed N³POM preserves the interpretability of the conventional POM and NPOM. We also provide a sufficient condition of the functions a, \mathbf{b} to satisfy the monotonicity constraint of the predicted CCP. Using this constraint, we propose a *monotonicity-preserving stochastic* (MPS) algorithm, that trains the parametric functions a, \mathbf{b} by maximizing the weighted log-likelihood via stochastic gradient ascent algorithm. Figure 1 illustrates the comparison of POM, NPOM, and N³POM (proposal). N³POM demonstrates better scores than existing POM and NPOM in synthetic dataset experiments. We apply N³POM to several real-world datasets.

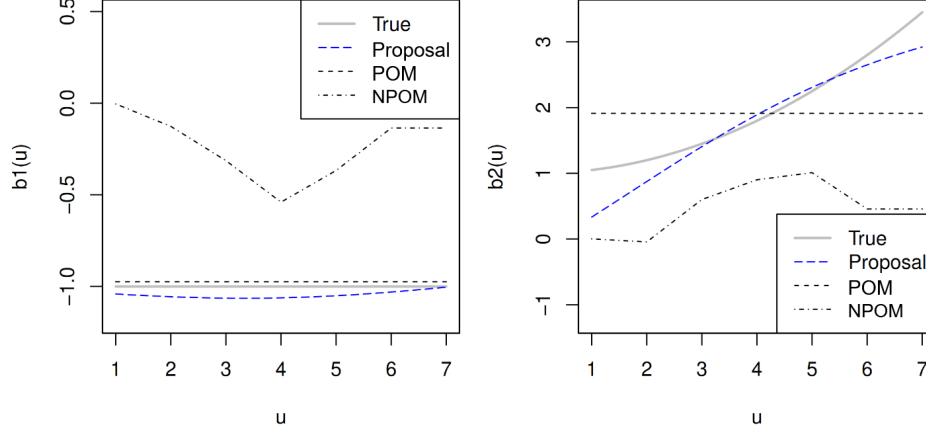


Figure 1: Illustration of N³POM. Grey lines represent the true coefficients $\mathbf{b}_*(u) = (b_{*1}(u), b_{*2}(u)) = (-1, 1 + 0.05u^2)$, blue lines represent the estimated coefficients $\hat{\mathbf{b}}(u)$ of the proposed N³POM, black lines represent the coefficients of existing POM implemented by `polr` function in R language, and NPOM implemented by `ordinalNet` function equipped with ridge penalty. Coefficients of POM and NPOM are linearly interpolated. This illustration corresponds to an instance in the synthetic dataset experiments. See Section 4 for details.

2 Preliminaries and Related Works

Section 2.1–2.3 summarize problem setting, symbols, and related works, respectively.

2.1 Problem setting

This section again describes the problem setting considered in this paper. Let $n, d, J \in \mathbb{N}$, and let $H \in \mathcal{U} := [1, J]$ be a random variable representing an ordered response associated with a covariate $X \in \mathbb{R}^d$. Let $\{(h_i, \mathbf{x}_i)\}_{i=1}^n \subset \mathcal{U} \times \mathbb{R}^d$ be n i.i.d. observations of the pair (H, X) . Then, using the observations, this study aims at predicting the conditional cumulative probability (CCP)

$$\mathbb{P}(H \leq u \mid X = \mathbf{x}), \quad (u \in \mathcal{U} = [1, J]), \quad (1)$$

(or equivalently, $\mathbb{P}(H > u \mid X = \mathbf{x})$) through ordinal logistic modeling. Particularly, the estimated CCP $\hat{\mathbb{P}}(H \leq u \mid X = \mathbf{x})$ is expected to be non-decreasing with respect to $u \in \mathcal{U}$, for fixed \mathbf{x} . Throughout this paper, the non-decreasing property is also referred to as monotonicity.

2.2 Symbols

This paper leverages the following symbols. $\sigma(z) = 1/(1 + \exp(-z))$ represents a sigmoid function. $\rho: \mathbb{R} \rightarrow \mathbb{R}$ denotes a user-specified activation function of the neural network (i.e., $\rho(z) = \tanh(z)$), and $\rho^{[1]}(z) = \rho(z)'$, $\rho^{[2]}(z) = \rho(z)''$ denote its first- and second-order derivatives. $\|\mathbf{x}\|_p = \{x_1^p + x_2^p + \dots + x_d^p\}^{1/p}$ for $\mathbf{x} = (x_1, x_2, \dots, x_d)$, $p \in \mathbb{N}$. $\langle \mathbf{x}, \mathbf{x}' \rangle = \mathbf{x}^\top \mathbf{x}'$ denotes an inner product of the vectors \mathbf{x}, \mathbf{x}' . \emptyset denotes an empty set.

For clarity, in this paper, ∇_θ, ∇_u are called by different names as the gradient (with respect to θ) and derivative (with respect to u), respectively. Particularly, for any function $f: \mathcal{U} \rightarrow \mathbb{R}$, $f^{[1]}: \mathcal{U} \rightarrow \mathbb{R}$ is called a weak derivative of f , if $f(u) = f(1) + \int_1^u f^{[1]}(\tilde{u}) d\tilde{u}$ holds for any $u \in \mathcal{U}$. If f is differentiable almost everywhere over \mathcal{U} , $f^{[1]}$ is compatible with $\nabla_u f(u)$ except for all the (non-measurable) indifferentiable points of f ; $f^{[1]}$ can be defined even if f is indifferentiable at some points. Note that the weak derivative of f is generally not unique, so we will define a weak derivative for each function.

2.3 Related works

Among several types of ordinal regression models, such as the continuation-ratio logit mode and the adjacent-categories logit model (Agresti, 2010), this paper focuses on the cumulative logit model.

In line with the ordinal regression, there are not many studies for a continuous response. Thas et al. (2012) proposes a probabilistic index model, which models the pairwise ordinal relationship $\mathbb{P}(H_i \leq H_j | X_i = \mathbf{x}_i, X_j = \mathbf{x}_j)$, and Liu et al. (2017) extends POM to a continuous response with a non-specific cumulative link function, though both of these studies assume parallel regression coefficients.

In other areas, survival analysis has much in common with ordinal regression with continuous response. One of the most widely-used approaches in survival analysis, leveraging the covariate X , is Cox's model. Cox's model is a semi-parametric function

$$\lambda_{\text{Cox}}(u | X = \mathbf{x}) = \lambda_0(u) \exp(\langle \boldsymbol{\gamma}_{\text{Cox}}(u), \mathbf{x} \rangle)$$

that approximates the hazard function:

$$\lambda(u | X = \mathbf{x}) := \frac{q(u | X = \mathbf{x})}{\mathbb{P}(H > u | X = \mathbf{x})} = -\frac{\frac{d}{du} \{1 - \mathbb{P}(H \leq u | X = \mathbf{x})\}}{1 - \mathbb{P}(H \leq u | X = \mathbf{x})} = -\frac{d}{du} \log \{1 - \mathbb{P}(H \leq u | X = \mathbf{x})\}, \quad (2)$$

where $u \geq 0$ is regarded as a time-point in survival analysis, and $\lambda_0(u)$ is a non-negative baseline-hazard function. While most of the standard Cox's model employs a constant coefficient (i.e., there exists a vector $\boldsymbol{\gamma}$ such that $\boldsymbol{\gamma}_{\text{Cox}}(u) = \boldsymbol{\gamma}$ for all u), we consider a response-dependent (non-constant) coefficient $\boldsymbol{\gamma}_{\text{Cox}}(u)$ for comparison. For such a flexible coefficient function, see, e.g., Hastie and Tibshirani (1993). Solving the differential equation (2) yields the CCP

$$\mathbb{P}_{\text{Cox}}(H \leq u | X = \mathbf{x}) = 1 - \exp\left(-\int_0^u \lambda_{\text{Cox}}(\tilde{u} | X = \mathbf{x}) d\tilde{u}\right) = 1 - \exp\left(-\int_0^u \lambda_0(\tilde{u}) \exp(\langle \boldsymbol{\gamma}_{\text{Cox}}(\tilde{u}), \mathbf{x} \rangle) d\tilde{u}\right). \quad (3)$$

However, compared to our model (5) defined later in Section 3.1, it is hard to interpret the coefficient $\boldsymbol{\gamma}_{\text{Cox}}(u)$ from the perspective of the CCP (3). As well, most survival analysis methods focus more on the hazard function estimation, rather than the estimation of CCP.

Regarding the CCP estimation leveraging the covariates, in the context of the survival analysis, Bennett (1983) defines a log-logistic regression model: $\mathbb{P}_{\text{Bennett}}(H \leq u | X = \mathbf{x}) = \sigma(a \log u + \langle \mathbf{b}, \mathbf{x} \rangle)$. While this model and its variants assume parallel regression coefficients \mathbf{b} (see, e.g., Kalbfleisch and Prentice (2002) for a comprehensive survey), Satoh et al. (2016) further modifies this simple model to

$$\mathbb{P}_{\text{Satoh}}(H \leq u | X = \mathbf{x}) = \sigma(a_{\text{Satoh}}(u) + \langle \mathbf{b}_{\text{Satoh}}(u), \mathbf{x} \rangle), \quad (4)$$

that is a closer model to ours. (4) is also called the time-varying coefficient model. Therein, the functions $a_{\text{Satoh}}, \mathbf{b}_{\text{Satoh}}$ are defined by polynomial functions

$$a_{\text{Satoh}}(u) = \sum_{\ell=1}^L u^{\ell-1} \tilde{a}_{\ell}, \quad \mathbf{b}_{\text{Satoh}}(u) := \sum_{\ell=1}^L u^{\ell-1} \tilde{\mathbf{b}}_{\ell},$$

where $\{\tilde{a}_{\ell}\}_{\ell=1}^L \subset \mathbb{R}$, $\{\tilde{\mathbf{b}}_{\ell}\}_{\ell=1}^L \subset \mathbb{R}^d$ are parameters to be estimated. However, unfortunately, any sufficient condition to guarantee the monotonicity of the model (4) is not provided in Satoh et al. (2016), while our model (5) is proved to be monotone when the covariate lies in the ball $\chi_2(\eta) := \{\mathbf{x} \in \mathbb{R}^d \mid \|\mathbf{x}\|_2 \leq \eta\}$ as discussed in Section 3.2. For counterexample of the monotonicity, (4) reduces to a function $\sigma(a_{\text{Satoh}}(u) + \langle \mathbf{b}_{\text{Satoh}}(u), \mathbf{x} \rangle) = \sigma((u-2)(u-3))$ not monotone with respect to $u > 0$ for all $\mathbf{x} \in \mathbb{R}^d$ (i.e., invalid as an estimator of CCP), by specifying $a_{\text{Satoh}}(u) = (u-2)(u-3)$ (i.e., $\tilde{a}_1 = 6, \tilde{a}_2 = -5, \tilde{a}_3 = 1, \tilde{a}_4 = \tilde{a}_5 = \dots = 0$) and $\mathbf{b}_{\text{Satoh}}(u) = \mathbf{0}$ (i.e., $\tilde{\mathbf{b}}_1 = \dots = \tilde{\mathbf{b}}_L = \mathbf{0}$).

3 Proposed Model

This section proposes a novel ordinal regression model for continuous response. We describe the proposed N³POM in Section 3.1, and we discuss the monotonicity of N³POM in Section 3.2. Using the above model endowed with the monotonicity, we provide a parameter estimation algorithm in Section 3.3. We last discuss the adaptation to the discrete responses in Section 3.4.

3.1 Neural network-based non-proportional odds model (N³POM)

To simultaneously address the difficulties (D-1) lack of the monotonicity of the predicted CCP, (D-2) lack of the proximity guarantee of the estimated coefficients for adjacent thresholds, and (D-3) lack of the extensibility to continuous responses, where they are explained in Introduction, we propose a *neural network-based non-proportional odds model* (N³POM):

$$\mathbb{P}_{\text{N}^3\text{POM}}(H \leq u \mid X = \mathbf{x}) = \sigma(\underbrace{a(u) + \langle \mathbf{b}(u), \mathbf{x} \rangle}_{=: f_u(\mathbf{x})}), \quad (u \in \mathcal{U} = [1, J]). \quad (5)$$

Continuous functions $a : \mathcal{U} \rightarrow \mathbb{R}$, $\mathbf{b} : \mathcal{U} \rightarrow \mathbb{R}^d$, and their weak derivatives $a^{[1]}, \mathbf{b}^{[1]}$ will be defined later in (7)–(10); using the weak derivative $f_u^{[1]}(\mathbf{x}) := a^{[1]}(u) + \langle \mathbf{b}^{[1]}(u), \mathbf{x} \rangle$, we obtain a conditional probability density (CPD) of $H \mid X$ as

$$q(u \mid X = \mathbf{x}) = \nabla_u \mathbb{P}_{\text{N}^3\text{POM}}(H \leq u \mid X = \mathbf{x}) = \sigma^{[1]}(f_u(\mathbf{x})) f_u^{[1]}(\mathbf{x}). \quad (6)$$

For preventing the non-negativity of the probability density, the prediction model $f_u(\mathbf{x})$ should be non-decreasing (with respect to $u \in \mathcal{U}$, for any fixed $\mathbf{x} \in \mathcal{X}$); we show a sufficient condition to guarantee the monotonicity in Section 3.2, and provide a parameter estimation algorithm in Section 3.3. Furthermore, in Section 3.4, we consider training N³POM even when only the discrete response is available. Note that estimating the CCP $\mathbb{P}_{\text{N}^3\text{POM}}(H \leq u \mid X = \mathbf{x}) = \sigma(f_u(\mathbf{x}))$ is also equivalent to estimating $\mathbb{P}_{\text{N}^3\text{POM}}(H > u \mid X = \mathbf{x}) = 1 - \mathbb{P}_{\text{N}^3\text{POM}}(H \leq u \mid X = \mathbf{x}) = 1 - \sigma(f_u(\mathbf{x})) = \sigma(-f_u(\mathbf{x}))$.

To complete the definition of N³POM, we define the parametric functions a, \mathbf{b} and their weak derivatives $a^{[1]}, \mathbf{b}^{[1]}$ in the remaining of this section.

- Regarding the function $a : \mathcal{U} \rightarrow \mathbb{R}$, this paper considers a piece-wise linear functions with user-specified $R \in \mathbb{N}$ and $1 = j_1 < j_2 < \dots < j_R = J$ (such that $\mathcal{U} = [j_1, j_R]$):

$$a(u) := \begin{cases} \alpha_r & (u = j_r, r \in \{1, 2, \dots, R\}) \\ \alpha_{r-1} + s_{r-1}(u - j_{r-1}) & (u \in (j_{r-1}, j_r), r \in \{2, 3, \dots, R\}) \end{cases}, \quad (7)$$

where $s_{r-1} := \frac{\alpha_r - \alpha_{r-1}}{j_r - j_{r-1}}$ denotes the slope of the line connecting two points (j_{r-1}, α_{r-1}) and (j_r, α_r) . $-\infty < \alpha_1 \leq \alpha_2 \leq \dots \leq \alpha_R < \infty$ are parameters to be estimated. This piece-wise linear function is non-decreasing and satisfying $a(j_r) = \alpha_r$ ($r \in \{1, 2, \dots, R\}$). Consider a disjoint division of the interval \mathcal{U} :

$$\mathcal{U}_{r-1} := \begin{cases} [j_{r-1}, j_r) & (r \in \{2, 3, \dots, R-1\}) \\ [j_{R-1}, j_R] & (r = R) \end{cases} \quad \text{satisfying} \quad \bigcup_{r=2}^R \mathcal{U}_{r-1} = \mathcal{U}, \mathcal{U}_r \cap \mathcal{U}_{r'} = \emptyset \ (r \neq r').$$

Then, we obtain a weak derivative:

$$a^{[1]}(u) := \sum_{r=2}^R \mathbb{1}(u \in \mathcal{U}_{r-1}) s_{r-1}. \quad (8)$$

- Regarding the vector-valued function $\mathbf{b}(u) = (b_1(u), b_2(u), \dots, b_d(u)) : \mathcal{U} \rightarrow \mathbb{R}^d$, we employ independent neural networks (NNs) $b_1, b_2, \dots, b_d : \mathcal{U} \rightarrow \mathbb{R}$ defined by

$$b_k(u) := v_k^{(2)} + \sum_{\ell=1}^L w_{k,\ell}^{(2)} \rho(w_{k,\ell}^{(1)} u + v_{k,\ell}^{(1)}), \quad (k \in \{1, 2, \dots, d\}), \quad (9)$$

where $\boldsymbol{\psi}_k := \{w_{k,\ell}^{(2)}, w_{k,\ell}^{(1)}, v_k^{(2)}, v_{k,\ell}^{(1)}\}_\ell$ is a set of weights to be estimated. As is well known, the neural network $\mathbf{b}(u)$ has a universal approximation capability, i.e., $\mathbf{b}(u)$ is capable of approximating any continuous function $\mathbf{b}_*(u)$ by increasing the number of hidden units $L \rightarrow \infty$ (see, e.g., [Cybenko \(1989\)](#)). $\rho : \mathbb{R} \rightarrow \mathbb{R}$ denotes an activation function. We generally assume that

$$(i) \rho \text{ is twice-differentiable, and } (ii) \rho_\infty^{[1]} := \sup_{z \in \mathbb{R}} |\rho(z)'| < \infty.$$

Sigmoid function $\rho(z) = 1/(1 + \exp(-z))$ and hyperbolic tangent function $\rho(z) = \tanh(z) := \{\exp(z) - \exp(-z)\} / \{\exp(z) + \exp(-z)\}$ satisfy these conditions (i) and (ii). Note that $b_k(u)$ reduces to a constant $v_k^{(2)}$ (which is independent of u) if $w_{k,\ell}^{(2)} = 0$ for all ℓ . Each entry of the derivative $\mathbf{b}^{[1]}(u) = (b_1^{[1]}(u), b_2^{[1]}(u), \dots, b_d^{[1]}(u))$ of the NN $\mathbf{b}(u)$ is

$$b_k^{[1]}(u) := \sum_{\ell=1}^L w_{k,\ell}^{(1)} w_{k,\ell}^{(2)} \rho^{[1]}(w_{k,\ell}^{(1)} u + v_{k,\ell}^{(1)}), \quad (k \in \{1, 2, \dots, d\}). \quad (10)$$

3.2 Monotonicity of N³POM

As the CCP $\mathbb{P}(H \leq u \mid X = \mathbf{x})$ should be non-decreasing with respect to $u \in \mathcal{U}$ (for any fixed $\mathbf{x} \in \mathcal{X}$), we consider the monotonicity of the N³POM (5). Equivalently, we focus on the monotonicity of the prediction model $f_u(\mathbf{x}) = a_u(\mathbf{x}) + \langle \mathbf{b}(u), \mathbf{x} \rangle$.

Firstly, we consider the function $a(u)$. As $f_u(\mathbf{0}) = a(u) + \langle \mathbf{b}(u), \mathbf{0} \rangle = a(u)$ should be monotone with respect to u , parameters in the function $a(u)$ are needed to satisfy the inequality

$$\alpha_1 \leq \alpha_2 \leq \dots \leq \alpha_R; \quad (11)$$

we employ a re-parameterization

$$\alpha_r = \alpha_r(\boldsymbol{\varphi}) = \begin{cases} \phi & (r = 1) \\ \phi + \sum_{t=2}^r |\varphi_t| & (r = 2, 3, \dots, R) \end{cases}, \quad (12)$$

equipped with newly-defined parameters $\boldsymbol{\varphi} = (\phi, \varphi_2, \varphi_3, \dots, \varphi_R) \in \mathbb{R}^R$ to be estimated. By virtue of the above re-parameterization, the monotonicity inequality (11) always holds.

Secondly, we consider the function $\mathbf{b}(u)$. Our interest is what types of the function $\mathbf{b}(u)$ can satisfy the monotonicity constraint in the sense of CCP. Unfortunately, however, we find that the function $\mathbf{b}(u)$ is limited to constant functions, if the N³POM is monotone for all the covariate \mathbf{x} in the unbounded, entire Euclidean space \mathbb{R}^d . See Proposition 1 with the proof shown in Appendix C.

Proposition 1. Let $a : \mathcal{U} \rightarrow \mathbb{R}$ be a function defined in (7), equipped with the re-parameterization (12). Let $\mathbf{b} : \mathcal{U} \rightarrow \mathbb{R}^d$ be a continuous function. If $f_u(\mathbf{x}) := a(u) + \langle \mathbf{b}(u), \mathbf{x} \rangle$ is non-decreasing with respect to $u \in \mathcal{U}$ for any fixed $\mathbf{x} \in \mathbb{R}^d$, $\mathbf{b}(u)$ is a constant function.

While N³POM cannot be monotone uniformly over the entire covariate Euclidean space, observed covariates are usually expected to distribute in a specific bounded region. Therefore, instead of the unbounded Euclidean space \mathbb{R}^d , we consider a closed ball region (i.e., a bounded region) for \mathbf{x} :

$$\mathcal{X}_2(\eta) := \{\mathbf{x} \in \mathbb{R}^d \mid \|\mathbf{x}\|_2 \leq \eta\}$$

equipped with a user-specified parameter $\eta > 0$, and prove that N³POM can be monotone for all the covariates $\mathbf{x} \in \mathcal{X}_2(\eta)$. A sufficient condition we provide for proving the monotonicity is satisfying an inequality

$$\min_{r=2,3,\dots,R} s_{r-1} \geq \eta \cdot \rho_\infty^{[1]} \cdot \sqrt{\sum_{k=1}^d \left\{ \sum_{\ell=1}^L |w_{k,\ell}^{(2)} w_{k,\ell}^{(1)}| \right\}^2}, \quad (13)$$

with $\rho_\infty^{[1]} := \max_{z \in \mathbb{R}} |\rho^{[1]}(z)|$. For instance, $\rho_\infty^{[1]} = 1/4$ for the sigmoid function $\rho(z) = 1/(1 + \exp(-z))$, and $\rho_\infty^{[1]} = 1$ for $\rho(z) = \tanh(z)$. $s_{r-1} := \{a_r - a_{r-1}\} / \{j_r - j_{r-1}\} = \varphi_r^2 / \{j_r - j_{r-1}\}$ represents a slope of the function $a(u)$. Then, the following proposition holds, with the proof shown in Appendix C. See Figure 2 for illustration.

Proposition 2. Let $a : \mathcal{U} \rightarrow \mathbb{R}$ be a function defined in (7), equipped with the re-parameterization (12). Let $\mathbf{b} : \mathcal{U} \rightarrow \mathbb{R}^d$ be a neural network defined in (9) for each element. Suppose the inequality (13) holds. Then, $f_u(\mathbf{x})$ is non-decreasing with respect to $u \in \mathcal{U}$, for any $\mathbf{x} \in \mathcal{X}_2(\eta)$.

Therefore, by specifying $\eta > \max_i \|\mathbf{x}_i\|_2$, the estimated CCP for all the observed covariates $\{\mathbf{x}_i\}_{i=1}^n$ satisfies the monotonicity as $\{\mathbf{x}_i\}_{i=1}^n \subset \mathcal{X}_2(\eta)$.

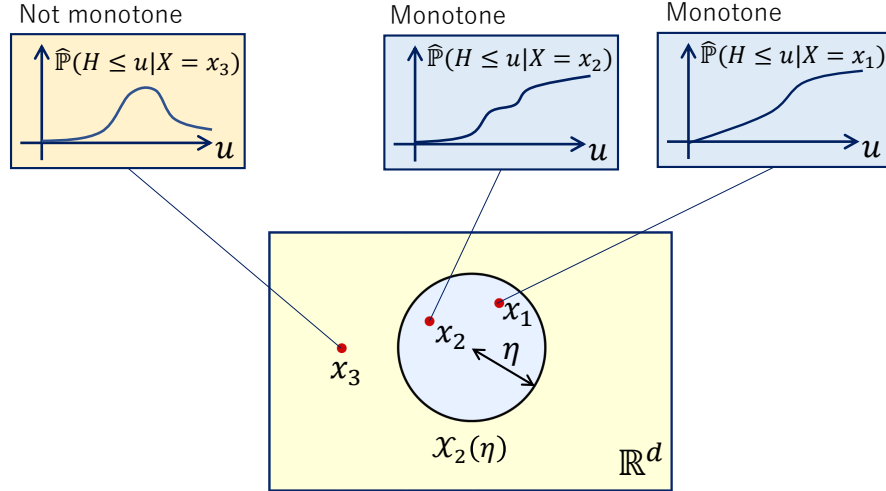


Figure 2: Illustration of Proposition 2. The estimated CCP $\hat{\mathbb{P}}_{\text{N}^3\text{POM}}(H \leq u \mid X = \mathbf{x}) = \sigma(\hat{f}_u(\mathbf{x}))$ is non-decreasing with respect to $u \in \mathcal{U}$ (i.e., valid) if $\mathbf{x} \in \mathcal{X}_2(\eta)$, while monotonicity is not guaranteed (i.e., invalid) if $\mathbf{x} \notin \mathcal{X}_2(\eta)$.

Here, we consider the relation to Proposition 1. Substituting $\eta = \infty$ (corresponding to $\mathcal{X}_2(\eta) = \mathbb{R}^d$) into the inequality (13) yields the identity $\max_{k,\ell} |w_{k,\ell}^{(2)} w_{k,\ell}^{(1)}| = 0$. Namely, $w_{k,\ell}^{(2)} = 0$ or $w_{k,\ell}^{(1)} = 0$ for all k, ℓ ; the function $b_k(u)$ then reduces to a constant function $b_k(u) = \sum_{\ell=1}^L w_{k,\ell}^{(2)} \sigma(v_{k,\ell}^{(1)}) + v_{k,\ell}^{(2)}$, as also indicated in Proposition 1. Conversely, specifying small η allows larger fluctuation of $\mathbf{b}(u)$ as the neural network weights $\{w_{k,\ell}^{(2)}, w_{k,\ell}^{(1)}\}$ can take larger values in the absolute value sense. Therefore, there exists a trade-off between the model flexibility and the area of the covariate region in which the CCP is monotone.

We last note that, to the best of the authors' knowledge, the unfavorable property we shed light on in Proposition 1 also holds for NPOM, though none of the existing studies explicitly mention this Proposition. Regarding the existing approaches in line with Tutz and Berger (2022), Lu et al. (2022), and Wurm et al. (2021), that penalize the distance between the coefficients and prototype $\|\boldsymbol{\beta}_j - \boldsymbol{\beta}_*\|$, increasing the penalty weight corresponds to decreasing η in our approach. Although they attempt to specify the penalty weights so that the CCP preserves the monotonicity over the observed covariates in the training dataset, they are not guaranteed to be monotone in the out-of-sample region.

3.3 Monotonicity-preserving stochastic (MPS) algorithm

Using the CPD $q(u | X = \mathbf{x})$ defined in (6), we propose a *monotonicity-preserving stochastic* (MPS) algorithm. MPS algorithm estimates the parameters of the prediction model $f_u(\mathbf{x}) = a(u) + \langle \mathbf{b}(u), \mathbf{x} \rangle$ by greedily maximizing the weighted log-likelihood:

$$\begin{aligned} \ell_{\zeta}(\boldsymbol{\theta}) &:= \sum_{i=1}^n \zeta_i \log q(h_i | X = \mathbf{x}_i) \\ &= \sum_{i=1}^n \zeta_i \{ \log \sigma^{[1]}(a(h_i) + \langle \mathbf{b}(h_i), \mathbf{x}_i \rangle) + \log(a^{[1]}(h_i) + \langle \mathbf{b}^{[1]}(h_i), \mathbf{x}_i \rangle) \}, \end{aligned} \quad (14)$$

under the sufficient condition constraint (13). $\zeta_i \geq 0$ ($i \in \{1, 2, \dots, n\}$) are user-specified weights satisfying $\sum_{i=1}^n \zeta_i = 1$ (e.g., $\zeta_1 = \zeta_2 = \dots = \zeta_n = 1/n$). (14) is a continuous variant of the log-likelihood used in conventional NPOM. See Remark 1.

With an initial parameter $\boldsymbol{\theta}^{(0)}$, the MPS algorithm repeats the following two steps for $t = 1, 2, \dots$ iteratively until convergence.

- (i) Compute a single step of the minibatch gradient ascent algorithm (Goodfellow et al., 2016) regarding the parameters $\boldsymbol{\varphi} = (\phi, \varphi_2, \dots, \varphi_R)$ for $a(u)$ and $\boldsymbol{\psi} = \{w_{k,\ell}^{(2)}, w_{k,\ell}^{(1)}, v_k^{(2)}, v_{k,\ell}^{(1)}\}$ for $\mathbf{b}(u)$. Explicit forms of the gradients for the gradient ascent are shown in Appendix A.

- (ii) With the coefficient

$$c = \min \left\{ 1, \frac{\min_{r=2,3,\dots,R} S_{r-1}}{\eta \cdot \rho_{\infty}^{[1]} \cdot \sqrt{\sum_{k=1}^d \left\{ \sum_{\ell=1}^L |w_{k,\ell}^{(2)} w_{k,\ell}^{(1)}| \right\}^2}} \right\},$$

we replace $w_{k,\ell}^{(2)}, w_{k,\ell}^{(1)}$ by $\sqrt{c} \cdot w_{k,\ell}^{(2)}, \sqrt{c} \cdot w_{k,\ell}^{(1)}$ so as to satisfy the inequality (13), that is a sufficient condition to guarantee the monotonicity of the predicted CCP.

Different from the standard minibatch gradient ascent algorithm (consisting of only step (i)), step (ii) is needed to guarantee the monotonicity of the predicted CCP $\hat{\mathbb{P}}_{\text{N}^3\text{POM}}(H \leq u | X = \mathbf{x})$, as discussed in Section 3.2.

Remark 1 (Relation to the likelihood of NPOM). Define a function $v_i(\Delta) = \{\mathbb{P}(H \leq h_i | X = \mathbf{x}_i) - \mathbb{P}(H \leq h_i - \Delta | X = \mathbf{x}_i)\} / \Delta$ (satisfying $\lim_{\Delta \searrow 0} v_i(\Delta) = q(h_i | X = \mathbf{x}_i)$) and $j_1 = 1, j_2 = 2, \dots, j_R = R = J$. Then, the log-likelihood (14) corresponds to $\sum_{i=1}^n \zeta_i \log \{\lim_{\Delta \searrow 0} v_i(\Delta)\}$ while the log-likelihood of the discrete NPOM is its discrete approximation $\sum_{i=1}^n \zeta_i \log v_i(1)$ (see, e.g., Peterson and Harrell (1990)).

3.4 Adaptation to the discrete responses

While we considered the response $H \in [1, J]$ taking a value in the connected interval $[1, J]$, it would be worthwhile to consider the adaptation to the discrete response $G \in \{1, 2, \dots, J\}$ due to the variety of applications. Although the proposed N^3POM (5) can be formally trained by leveraging the discrete response, the discrete responses are not sufficient to fully train the continuous model $f_u(\mathbf{x})$. Experimentally speaking, using several synthetic and real-world datasets, N^3POM trained with the discrete response behaves similarly to POM model (i.e., the estimated coefficients $\mathbf{b}(u)$ reduce to a constant) even if the underlying function is response-dependent. To solve this issue, we propose to incorporate an additive perturbation to the responses so that the responses take values in not only $\{1, 2, \dots, J\}$ but the connected interval $[1, J]$.

Our idea is simple. If we have the discrete responses $g_1, g_2, \dots, g_n \in \{1, 2, \dots, J\}$, we generate the random numbers e_1, e_2, \dots, e_n i.i.d. uniformly over the region $[-0.5, 0.5]$, and adding the e_1, e_2, \dots, e_n to

g_1, g_2, \dots, g_n , respectively. Finally, we round the obtained responses to take values in between 1 and J . Namely, we define a (random) perturbation operator

$$\mathfrak{C}(g_i) := \operatorname{argmin}_{j \in [1, J]} |(g_i + e_i) - j|, \quad (i \in \{1, 2, \dots, n\}). \quad (15)$$

Although heuristic, this perturbation operator (15) is explainable in the context of ordinary least squares regression. As is well known in asymptotic theory, the estimated regression function in ordinary least squares converges to the conditional expectation $f_*(X) = \mathbb{E}[G | X]$; so adding the mean-zero perturbation $E \sim U[-0.5, 0.5]$ is expected not to cause any bias (i.e., $\mathbb{E}[G + E | X] = \mathbb{E}[G | X] = f_*(X)$). A similar result is expected to hold for ordinal regression. While the estimation efficiency slightly decreases by this perturbation, there also exists an advantage to fully training the continuous NN; see numerical experiments in Section 4 for the effectiveness of the additive perturbation (15).

Table 1: Results of MSE experiments on synthetic datasets, where the observed covariates are generated by the setting (i) $x_i = (r_i \cos \theta_i, r_i \sin \theta_i)$, $r_i \sim U([0, 1])$, $\theta_i \sim U([0, 2\pi))$. Among 30 experiments for each setting, the median and standard deviation (shown in parenthesis) are computed. The best score is **bolded and blue-colored**, and the second best score is **bolded and red-colored**

(a) Both coefficients $b_{*1}(u) = -1 + m_1 u^2$, $b_{*2}(u) = 1 + m_2 u^2$ are response-dependent (i.e., not constant).

Model	Optimizer	Response	$(m_1, m_2) = (0.05, -0.05)$		$(m_1, m_2) = (0.05, 0.05)$	
			MSE(\hat{b}_1)	MSE(\hat{b}_2)	MSE(\hat{b}_1)	MSE(\hat{b}_2)
N ³ POM	MPS	h_i	0.066 (0.158)	0.120 (0.152)	0.056 (0.098)	0.176 (0.148)
N ³ POM	MPS	$\mathfrak{C}([h_i])$	0.116 (0.101)	0.162 (0.092)	0.094 (0.086)	0.204 (0.134)
N ³ POM	MPS	$[h_i]$	0.516 (0.061)	0.531 (0.034)	0.522 (0.049)	0.529 (0.053)
POM	polr	$[h_i]$	0.516 (0.024)	0.514 (0.022)	0.514 (0.031)	0.524 (0.030)
NPOM	(ridge) oNet	$[h_i]$	0.230 (0.041)	0.234 (0.080)	0.358 (0.029)	2.575 (0.169)
NPOM	(elastic) oNet	$[h_i]$	0.220 (0.184)	0.292 (0.197)	0.200 (0.078)	0.191 (0.119)
NPOM	(lasso) oNet	$[h_i]$	0.203 (0.197)	0.273 (0.205)	0.212 (0.100)	0.205 (0.179)
NPOM	serp	$[h_i]$	0.174 (0.075)	0.195 (0.086)	0.130 (0.073)	0.216 (0.091)

(b) At least either of $b_{*1}(u) = -1 + m_1 u^2$, $b_{*2}(u) = 1 + m_2 u^2$ is a constant function, i.e., $m_1 = 0$ or $m_2 = 0$.

Model	Optimizer	Response	$(m_1, m_2) = (0.05, 0)$		$(m_1, m_2) = (0, 0)$	
			MSE(\hat{b}_1)	MSE(\hat{b}_2)	MSE(\hat{b}_1)	MSE(\hat{b}_2)
N ³ POM	MPS	h_i	0.098 (0.193)	0.074 (0.055)	0.051 (0.051)	0.050 (0.074)
N ³ POM	MPS	$\mathfrak{C}([h_i])$	0.114 (0.147)	0.047 (0.046)	0.048 (0.072)	0.035 (0.064)
N ³ POM	MPS	$[h_i]$	0.521 (0.049)	0.010 (0.023)	0.005 (0.024)	0.009 (0.018)
POM	polr	$[h_i]$	0.512 (0.027)	0.003 (0.019)	0.008 (0.018)	0.003 (0.017)
NPOM	(ridge) oNet	$[h_i]$	0.321 (0.050)	0.533 (0.065)	0.551 (0.054)	0.561 (0.051)
NPOM	(elastic) oNet	$[h_i]$	0.217 (0.120)	0.178 (0.168)	0.231 (0.127)	0.176 (0.150)
NPOM	(lasso) oNet	$[h_i]$	0.212 (0.123)	0.218 (0.184)	0.232 (0.144)	0.221 (0.157)
NPOM	serp	$[h_i]$	0.186 (0.089)	0.026 (0.055)	0.013 (0.023)	0.019 (0.039)

4 Experiments on Synthetic Datasets

This section provides numerical experiments using synthetic datasets.

Table 2: Results of MSE experiments on synthetic datasets, where the observed covariates are generated by the setting (ii) $\mathbf{x}_i \sim U([0, 1]^2)$. Among 30 experiments for each setting, the median and standard deviation (shown in parenthesis) are computed. The best score is **bolded and blue-colored**, and the second best score is **bolded and red-colored**

(a) Both coefficients $b_{*1}(u) = -1 + m_1 u^2$, $b_{*2}(u) = 1 + m_2 u^2$ are response-dependent (i.e., not constant).

Model	Optimizer	Response	$(m_1, m_2) = (0.05, -0.05)$		$(m_1, m_2) = (0.05, 0.05)$	
			MSE(\hat{b}_1)	MSE(\hat{b}_2)	MSE(\hat{b}_1)	MSE(\hat{b}_2)
N ³ POM	MPS	h_i	0.219 (0.142)	0.191 (0.093)	0.229 (0.167)	0.234 (0.141)
N ³ POM	MPS	$[h_i]$	0.278 (0.098)	0.277 (0.107)	0.294 (0.131)	0.275 (0.120)
N ³ POM	MPS	$\mathfrak{C}([h_i])$	0.551 (0.075)	0.520 (0.039)	0.516 (0.026)	0.524 (0.027)
POM	polr	$[h_i]$	0.517 (0.026)	0.523 (0.018)	0.524 (0.024)	0.512 (0.025)
NPOM	(ridge) oNet	$[h_i]$	0.256 (0.085)	0.232 (0.071)	0.424 (0.032)	3.092 (0.089)
NPOM	(elastic) oNet	$[h_i]$	0.371 (0.234)	0.315 (0.202)	0.377 (0.162)	1.086 (0.797)
NPOM	(lasso) oNet	$[h_i]$	0.399 (0.306)	0.308 (0.242)	0.402 (0.210)	1.478 (0.890)
NPOM	serp	$[h_i]$	0.238 (0.108)	0.204 (0.071)	0.259 (0.192)	0.303 (0.148)

(b) At least either of $b_{*1}(u) = -1 + m_1 u^2$, $b_{*2}(u) = 1 + m_2 u^2$ is a constant function, i.e., $m_1 = 0$ or $m_2 = 0$.

Model	Optimizer	Response	$(m_1, m_2) = (0.05, 0)$		$(m_1, m_2) = (0, 0)$	
			MSE(\hat{b}_1)	MSE(\hat{b}_2)	MSE(\hat{b}_1)	MSE(\hat{b}_2)
N ³ POM	MPS	h_i	0.249 (0.147)	0.067 (0.084)	0.059 (0.062)	0.050 (0.064)
N ³ POM	MPS	$[h_i]$	0.296 (0.124)	0.026 (0.050)	0.029 (0.035)	0.030 (0.039)
N ³ POM	MPS	$\mathfrak{C}([h_i])$	0.521 (0.047)	0.014 (0.032)	0.010 (0.077)	0.029 (0.064)
POM	polr	$[h_i]$	0.513 (0.013)	0.004 (0.027)	0.010 (0.016)	0.012 (0.031)
NPOM	(ridge) oNet	$[h_i]$	0.389 (0.057)	0.512 (0.058)	0.517 (0.075)	0.479 (0.066)
NPOM	(elastic) oNet	$[h_i]$	0.408 (0.233)	0.325 (0.170)	0.230 (0.165)	0.137 (0.110)
NPOM	(lasso) oNet	$[h_i]$	0.450 (0.310)	0.332 (0.200)	0.254 (0.193)	0.148 (0.171)
NPOM	serp	$[h_i]$	0.301 (0.118)	0.029 (0.079)	0.021 (0.121)	0.023 (0.118)

4.1 Synthetic datasets

In this experiment, we set $n = 1000, d = 2, J = 7$. For the covariate X , we employ two different settings (i) and (ii): (i) we generate $r_1, r_2, \dots, r_n \sim U([0, 1])$ and $\theta_1, \theta_2, \dots, \theta_n \sim U([0, 2\pi])$ uniformly randomly, and compute $\mathbf{x}_i = (r_i \cos \theta_i, r_i \sin \theta_i) \in \mathbb{R}^2$, (ii) we generate $\mathbf{x}_i \sim U([0, 1]^2)$ i.i.d. uniformly randomly. We consider functions $a_*(u) = 2u - 9$ and

$$\mathbf{b}_*(u) = (b_{*1}(u), b_{*2}(u)) = (-1 + m_1 u^2, 1 + m_2 u^2)$$

so that the continuous responses h_1, h_2, \dots, h_n are generated from the conditional distribution $\mathbb{P}(H \leq h_i \mid X = \mathbf{x}_i) = \sigma(a_*(h_i) + \langle \mathbf{b}_*(h_i), \mathbf{x}_i \rangle)$. We further truncate u so as to take values in the interval $\mathcal{U} = [1, J]$ (by the function $\arg \min_{\tilde{u} \in [1, J]} \|u - \tilde{u}\|$), with $J = 7$. (Note that, the randomly generated u rarely gets out of the interval $[1, 7]$ in this setting). The covariates $\mathbf{x}_1, \mathbf{x}_2, \dots, \mathbf{x}_n$ lie in the unit disk $\mathcal{X}_2(1) = \{\mathbf{x} \in \mathbb{R}^2 \mid \|\mathbf{x}\|_2 \leq 1\}$; the underlying function $f_u(\mathbf{x}) = a_*(u) + \langle \mathbf{b}_*(u), \mathbf{x} \rangle$ is non-decreasing with respect to $u \in \mathcal{U}$ for all $\mathbf{x} \in \mathcal{X}_2(1)$, as $f_u^{[1]}(\mathbf{x}) = \nabla_u f_u(\mathbf{x}) = 2 - 2m_1 u x_1 + 2m_2 u x_2 \geq 0$.

To compute the baselines, we discretize the continuous responses h_i as

$$[h_i] := \arg \min_{j \in \{1, 2, \dots, J\}} \|h_i - j\|_2; \quad (16)$$

we train POM and NPOM by leveraging $[h_i]$. Furthermore, we train the proposed N³POM with $h_i, [h_i]$ and $\mathfrak{C}([h_i])$ for comparison purposes, where $\mathfrak{C}(\cdot)$ is the random perturbation operator defined in (15).

4.2 Experimental settings

Model architecture: we employ the proposed N^3POM (5) defined in Section 3.1. We specify $R = 16$ for the function $a(u)$ and we employ the regular intervals $j_1 = 1 < j_2 < j_3 < \dots < j_{16} = 7$. The number of hidden units of the neural network $b(u)$ is $L = 50$. Sigmoid activation function $\rho(z) = 1/(1 + \exp(-z))$ is employed.

Initialization: we first compute the coefficient vectors $\hat{\beta}_1, \hat{\beta}_2, \dots, \hat{\beta}_{j-1}$ of discrete NPOM, by leveraging `serp` package in R language. Then, we initialize the neural network parameters so that the NN outputs approximate the `serp` outputs over the discrete points (i.e., $b_k(j) \approx \hat{\beta}_{jk}$). See Appendix B for details. The parameters of the function $a(u)$ are also parameterized by linear interpolation of `serp` outputs.

Optimization: we compute a minibatch gradient ascent algorithm (Goodfellow et al., 2016) for maximizing the log-likelihood (14). The weights are specified as $w_i \propto 1/n_{r_i}^{0.5}$, where $n_r := |\{i : g_i \in \mathcal{U}_r\}|$ and $g_i \in \mathcal{U}_{r_i}$. A minibatch of size 16 is uniformly randomly selected from training samples (without replacement), and the number of iterations is 5000. The learning rate is multiplied by 0.95 for each 50 iteration. Using these settings, we apply the MPS algorithm to three types of responses: $h_i, \mathcal{C}([h_i]), [h_i]$.

Baselines: we employ two major implementations of ordinal regression: `polr` function (using a logistic model) in MASS package, and `ordinalNet` (`oNet`) function (using only non-parallel terms, cumulative logit, and a hyperparameter $\alpha \in \{0, 0.5, 1\}$) in `ordinalNet` package, in R language. We also employ `serp` function (using logit link and “penalize” slope option) in `serp` package (Ugba et al., 2021); `polr`, `ordinalNet`, `serp` are used for training POM, NPOM, and NPOM, respectively. As `ordinalNet` penalizes the coefficients as $\sum_{j=1}^{J-1} \{\alpha \|\beta_j\|_1 + (1 - \alpha) \|\beta_j\|_2^2\}$, $\alpha = 0, 0.5$ and 1 represent ridge, elastic, and lasso penalties, respectively. `serp` penalizes the adjacent coefficients $\|\beta_j - \beta_{j-1}\|_2^2$. The above baselines are applied to the discretized responses $[h_i]$.

Evaluation: for each estimated coefficient $\hat{b}_k(u)$, we compute mean squared error (MSE):

$$\text{MSE}(\hat{b}_k) := \frac{1}{|\tilde{\mathcal{U}}|} \sum_{\tilde{u} \in \tilde{\mathcal{U}}} \{b_{*k}(\tilde{u}) - \hat{b}_k(\tilde{u})\}^2 \quad (k = 1, 2),$$

with $\tilde{\mathcal{U}} := \{1, 1.05, 1.1, 1.15, 1.2, \dots, J\}$. For evaluating POM and discrete NPOM, we employ linear interpolation for computing $\hat{b}_k(u)$ for non-integer u . We compute the MSE for each of 30 times experiments; for robustly estimating the MSE, we compute their median for each setting. We also compute the standard deviation of MSE after removing the best and worst MSE for each setting.

4.3 Results

Setting(i). Experimental results for the covariate setting (i) $\mathbf{x}_i = (r_i \cos \theta_i, r_i \sin \theta_i)$, $r_i \sim U([0, 1])$, $\theta_i \sim U([0, 2\pi))$ are summarized in Table 1. For the response-dependent coefficients shown in Table 1(a), for all the cases, N^3POM trained with the continuous response h_i shows the best scores. N^3POM applied to the discretized response $[h_i]$ shows the scores nearly equal to `polr`. Even if the response is discretized, the score gets closer to that with the continuous response by leveraging the adaptation to the discrete responses shown in Section 3.4. Scores of NPOM implemented by `serp` package follow the scores of N^3POM . `ordinalNet` demonstrates the subsequent scores.

We also evaluate the proposed method and baselines, when either of the coefficients is a constant (i.e., $m_1 = 0$ or $m_2 = 0$) in Table 1(b). Similarly to the case of response-dependent coefficients, N^3POM trained with the discretized response demonstrates a similar score to POM using `polr` package (though we initialized the neural network using `serp` package). For the constant coefficients (corresponding to $m_1 = 0$

or $m_2 = 0$), POM and N^3 POM trained with the discrete responses demonstrates the best and second-best scores. This is because, the POM assumes the constant coefficients, so the estimation variance is much smaller than more flexible models NPOM and N^3 POM.

Setting (ii). Experimental results for the covariate setting (ii) $\mathbf{x}_i \sim U([0, 1]^2)$ are summarized in Table 2. Overall tendency is the same as the setting (i); N^3 POM trained with the continuous response h_i demonstrates best scores for estimating all of the non-constant coefficients, while POM and N^3 POM trained with the discrete response $[h_i]$ demonstrate the best scores for estimating the constant coefficients.

5 Experiments on Real-World Datasets

In this section, we train N^3 POM by leveraging real-world datasets. We show and interpret the results of the experiments for autoMPG6, autoMPG8, and real-estate datasets, while we also show the results of boston-housing, concrete, and airfoil datasets. We describe the experimental settings.

5.1 Real-world datasets

We employ the following datasets collected from UCI machine learning repository (Dua and Graff, 2017).

autoMPG6 ($n = 392, d = 5$) and **autoMPG8** ($n = 392, d = 7$). autoMPG6 dataset consists of 5 covariates (“Displacement” (continuous), “Horse power” (continuous), “Weight” (continuous), “Acceleration” (continuous), “Model year” (discrete)) and the continuous response “mpg”. “mpg” stands for miles per gallon, that represents the fuel efficiency. autoMPG8 dataset is an extension of autoMPG6, where the additional 2 covariates (“Cylinders” (discrete), “Origin”(discrete)) are incorporated. The remaining 5 covariates and the response are the same as autoMPG6. Although these datasets are almost the same, we can examine whether the estimated coefficients are robust against the newly additional covariates, by comparing N^3 POM trained with these datasets.

real-estate ($n = 413, d = 3$). Among 6 covariates in the original real-estate dataset, we first remove the covariates “X1:transaction date”, “X5:latitude”, “X6:longitude”, and we employ the remaining three covariates “X2:house.age”, “X3:distance.to.the.nearest.MRT.station”, “X4:number.of.convinience.stores”. They are renamed to “house age”, “Dist. to station”, “Num. of conv. stores” in our experiments. The response variable represents the house price of unit area, so we rename this variable as “house price oua”. For meaningful computation, we removed the 271st column, as its observed response is an outlier whose difference to the mean of the remaining responses are farther than 6 times of the standard deviation.

For each dataset, covariates are standardized (centering and scaling). Responses are linearly transformed so that $\min_i h_i = 1, \max_i h_i = 10$ (i.e., we set $J = 10$), and after computing N^3 POM, we recover the original response for plot by applying the inverse linear transformation. Also, see Supplement D for N^3 POM applied to boston-housing ($n = 502, d = 12$), concrete ($n = 1030, d = 8$), and airfoil ($n = 1503, d = 5$) datasets, and Supplement E for pairwise scatter plots of the covariates in these datasets.

5.2 Experimental settings

Initialization and optimization are the same as the experiments in Section 4, while we employ $R = 20$ with equal intervals $1 = j_1 < j_2 < \dots < j_R = J = 10$ in real-world dataset experiments.

We first compute `serp` function by leveraging the rounded responses $[h_i]$. Initialized by this `serp` output (see Appendix B), we train the neural network by the MPS algorithm. For considering the randomness to choose minibatches, in each plot, we compute 10 different stochastic optimization results.

For comparison, we also plot the initial neural network (approximating the preliminarily computed `serp` output) and the POM coefficients trained by `polr` function.

5.3 Results

Estimated coefficients for each dataset are shown in Figures 3–6. For interpretation, we inverse the sign of the estimated coefficients $\hat{\mathbf{b}}(u)$ as we have a probability that the response exceeds a threshold value u :

$$\hat{\mathbb{P}}_{\text{N}^3\text{POM}}(H > u \mid X = \mathbf{x}) = 1 - \hat{\mathbb{P}}_{\text{N}^3\text{POM}}(H \leq u \mid X = \mathbf{x}) = \sigma(-\hat{f}_u(\mathbf{x})) = \sigma(\hat{r}(u) + \langle \hat{\mathbf{s}}(u), \mathbf{x} \rangle)$$

with $\hat{r}(u) = -\hat{a}(u)$ and

$$\hat{\mathbf{s}}(u) = (\hat{s}_1(u), \hat{s}_2(u), \dots, \hat{s}_d(u)) = -\hat{\mathbf{b}}(u).$$

Therefore, the larger $\hat{s}_k(u) = -\hat{b}_k(u)$ (corresponding to smaller $\hat{b}_k(u)$) indicates larger response if the corresponding observed covariate is large.

autoMPG6 and autoMPG8. Firstly, we consider the results of autoMPG6 ($n = 392, d = 5$) and autoMPG8 ($n = 392, d = 7$) datasets shown in Figures 3 and 4, respectively. While the autoMPG8 dataset includes the additional two covariates “Cylinders” and “Origin”, the tendency of the estimated coefficients $\hat{s}_k(u)$ of the 5 common covariates (“Displacement”, “Horse power”, “Weight”, “Acceleration”, “Model year”) is almost the same for these two datasets. Regarding these 5 common covariates, coefficients $\hat{s}_k(u)$ of “Displacement”, “Horse power”, “Weight” are negative and decreasing; so taking higher displacement (or horse power/weight) indicates lower fuel efficiency, and they adversely affect the fuel efficiency more negatively for highly efficient cars. The remaining covariates $\hat{s}_k(u)$ for “Acceleration” and “Model year” are increasing; so increasing these values indicate higher fuel efficiency, and their importance also increases for highly efficient cars.

real-estate. Results of real-estate ($n = 413, d = 3$) dataset is shown in Figure 5(a). For the second covariate “Dist. to station”, the increasing distance adversely affects the house price, and the degree of the adverse effect increases for more expensive houses. The third covariate, “Number of convenience stores” positively affects the house price. However, the degree of the positive effect decreases for more expensive houses. For the first covariate “House age”, the house age adversely affects the house price for lower price houses, though the effect almost vanishes (as $\hat{s}_1(u)$ approaches 0 as u increases) for higher price houses. Also see Figure 5(b) for the scatter plots between covariates and the house price; for instance, we can observe that the house age does not seem to adversely affect the house price for higher price houses, while it seems to have a slightly negative effect when considering the lower price houses.

The regression results of several datasets are also provided in Supplement D. Also see Supplement E for pairwise scatter plots of all the datasets used in this paper.

6 Conclusion

We proposed a continuous neural network-based non-proportional odds model (N³POM) for ordinal regression. In our model, we computed the linear coefficients of ordinal regression by the neural network taking the ordinal and continuous response as its input. By virtue of the neural network, the estimated coefficients might have flexibility while preserving the interpretability of the conventional ordinal regression models. We showed a sufficient condition to preserve the monotonicity of the predicted conditional cumulative probabilities; we also provided an MPS algorithm for training the neural network adequately. N³POM demonstrated better scores than existing ones in synthetic dataset experiments, and we trained N³POM using several real-world datasets.

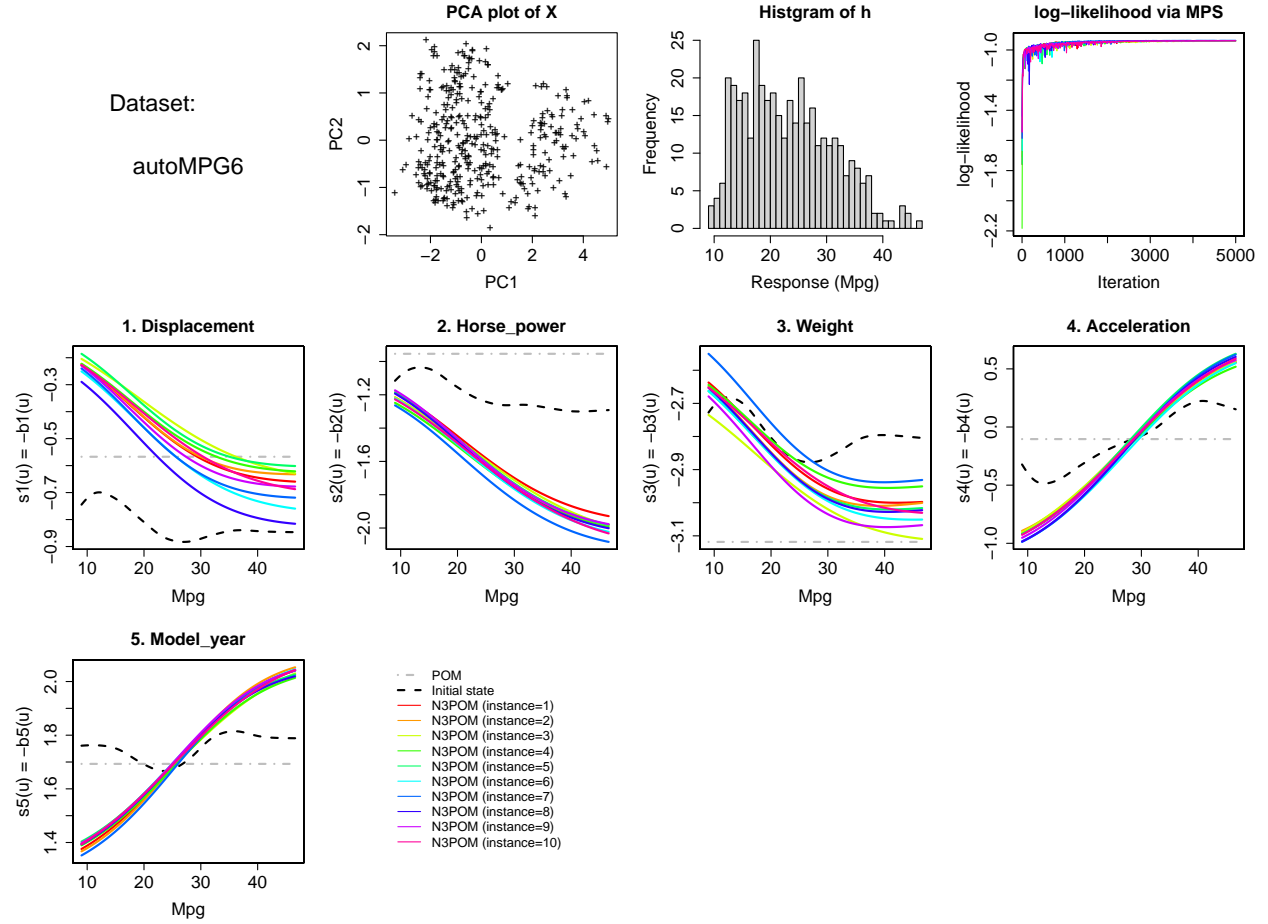


Figure 3: autoMPG6 dataset experiment.

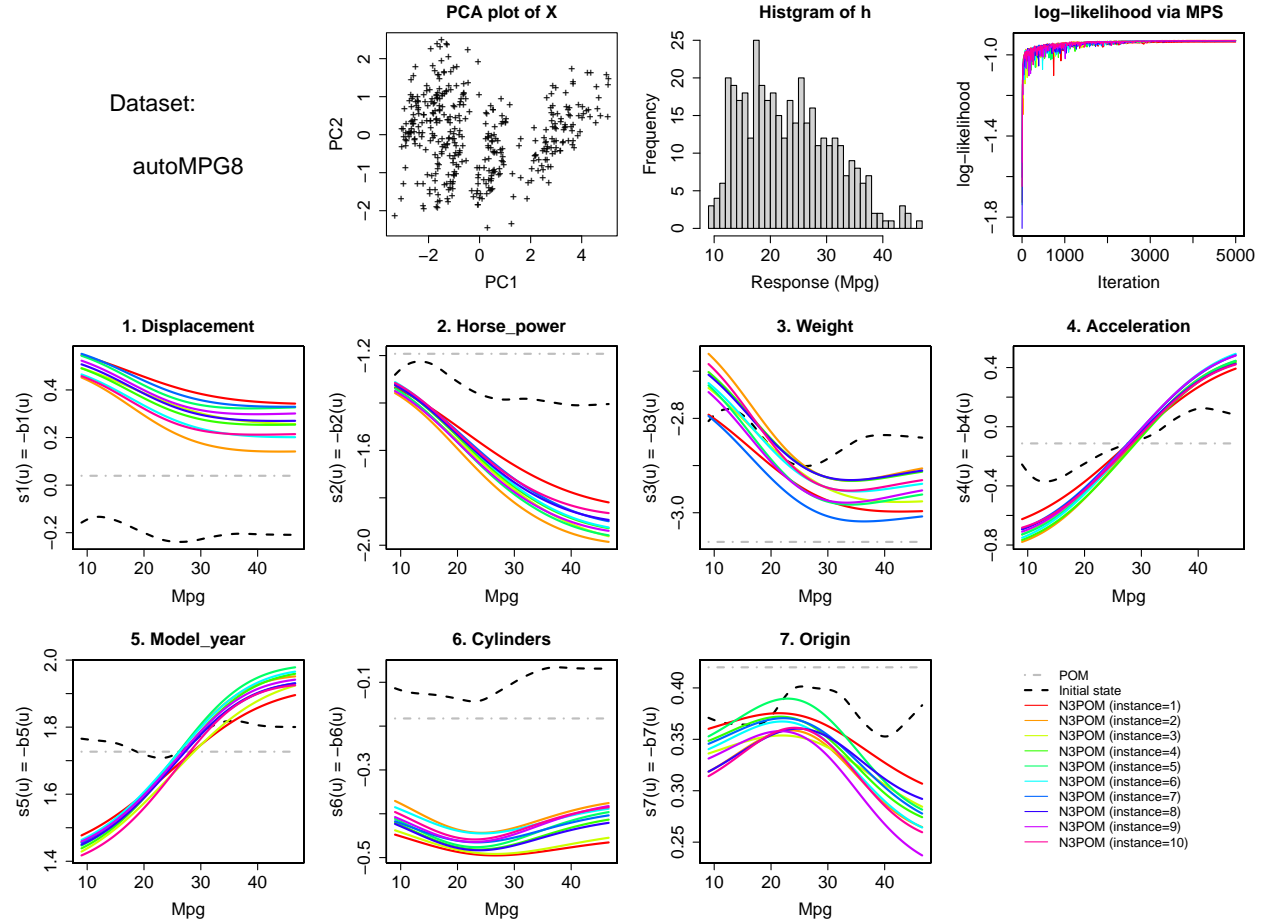
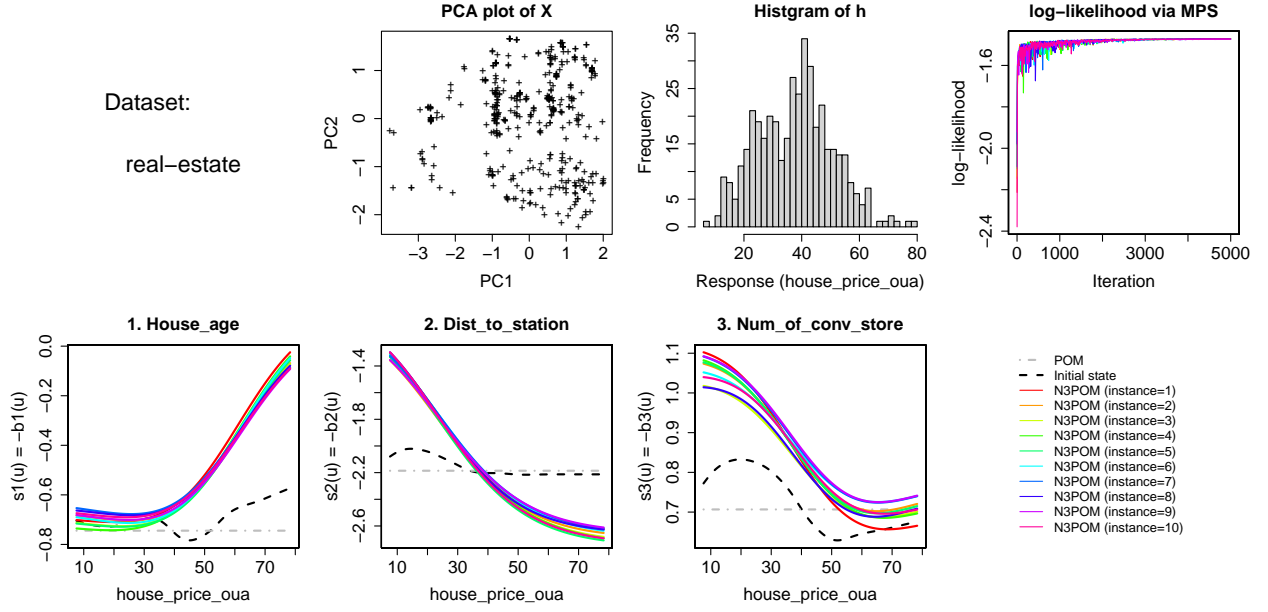
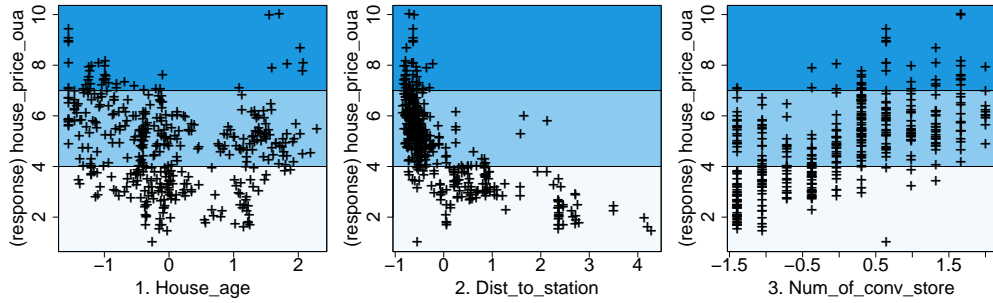


Figure 4: autoMPG8 dataset experiment.



(a) Experimental results.



(b) Scatter plots between covariates (house age, distance to station, and the number of stores; x -axis) and response (house price of unit area; y -axis). Higher price, middle price, and lower price houses are colored separately.

Figure 5: real-estate dataset.

Acknowledgement

A. Okuno was supported by JST CREST (JPMJCR21N3) and JSPS KAKENHI (21K17718, 22H05106). K. Harada was supported by JSPS KAKENHI (21J10457). We would like to thank Keisuke Yano, Kohei Hattori, Shuichi Kawano, and Kei Hirose, for helpful discussions.

A Gradient

With respect to the parameter θ , gradients $\nabla_{\theta} f_u, \nabla_{\theta} f_u^{[1]}$ of the prediction model f_u and its weak derivative $f_u^{[1]}$ are shown in Appendix A.1, A.2, respectively; together with these gradients, we show the gradient of the log-likelihood in Appendix A.3.

A.1 Gradient of the regression model

Let

$$\llbracket z \rrbracket = \begin{cases} 0 & (z < 0) \\ z & (z \in [0, 1]) \\ 1 & (z > 1) \end{cases}, \quad z \in \mathbb{R}.$$

Considering the identity

$$a(u) = \phi + \sum_{r=2}^R |\varphi_r| \left\llbracket \frac{u - j_{r-1}}{j_r - j_{r-1}} \right\rrbracket,$$

the gradient $\nabla_{\theta} f_u(\mathbf{x}_i)$ is obtained element-wise as: for $r^{\dagger} \in \{2, 3, \dots, R\}, k^{\dagger} \in [d], \ell^{\dagger} \in [L]$ and $u \in \mathcal{U}$,

$$\begin{aligned} \frac{\partial}{\partial \phi} f_u(\mathbf{x}_i) &= 1, \\ \frac{\partial}{\partial \varphi_{r^{\dagger}}} f_u(\mathbf{x}_i) &= \text{sign}(\varphi_{r^{\dagger}}) \left\llbracket \frac{u - j_{r^{\dagger}-1}}{j_{r^{\dagger}} - j_{r^{\dagger}-1}} \right\rrbracket, \\ \frac{\partial}{\partial v_{k^{\dagger}, \ell^{\dagger}}^{(1)}} f_u(\mathbf{x}_i) &= x_{ik^{\dagger}} \frac{\partial}{\partial v_{k^{\dagger}, \ell^{\dagger}}^{(1)}} b_{k^{\dagger}}(u) = x_{ik^{\dagger}} w_{k^{\dagger}, \ell^{\dagger}}^{(2)} \rho^{[1]}(w_{k^{\dagger}, \ell^{\dagger}}^{(1)} u + v_{k^{\dagger}, \ell^{\dagger}}^{(1)}), \\ \frac{\partial}{\partial v_{k^{\dagger}}^{(2)}} f_u(\mathbf{x}_i) &= x_{ik^{\dagger}} \frac{\partial}{\partial v_{k^{\dagger}}^{(2)}} b_{k^{\dagger}}(u) = x_{ik^{\dagger}}, \\ \frac{\partial}{\partial w_{k^{\dagger}, \ell^{\dagger}}^{(1)}} f_u(\mathbf{x}_i) &= x_{ik^{\dagger}} \frac{\partial}{\partial w_{k^{\dagger}, \ell^{\dagger}}^{(1)}} b_{k^{\dagger}}(u) = x_{ik^{\dagger}} w_{k^{\dagger}, \ell^{\dagger}}^{(2)} u \rho^{[1]}(w_{k^{\dagger}, \ell^{\dagger}}^{(1)} u + v_{k^{\dagger}, \ell^{\dagger}}^{(1)}), \\ \frac{\partial}{\partial w_{k^{\dagger}, \ell^{\dagger}}^{(2)}} f_u(\mathbf{x}_i) &= x_{ik^{\dagger}} \frac{\partial}{\partial w_{k^{\dagger}, \ell^{\dagger}}^{(2)}} b_{k^{\dagger}}(u) = x_{ik^{\dagger}} \rho(w_{k^{\dagger}, \ell^{\dagger}}^{(1)} u + v_{k^{\dagger}, \ell^{\dagger}}^{(1)}). \end{aligned}$$

A.2 Gradient of the weak derivative of the prediction model

Considering the identities

$$a^{[1]}(u) = \sum_{r=2}^R \mathbb{1}(u \in \mathcal{U}_{r-1}) \frac{|\varphi_r|}{j_r - j_{r-1}}, \quad b_k^{[1]}(u) = \sum_{\ell=1}^L w_{k, \ell}^{(2)} w_{k, \ell}^{(1)} \rho^{[1]}(w_{k, \ell}^{(1)} u + v_{k, \ell}^{(1)}),$$

the gradient $\nabla_{\theta} f_u^{[1]}(\mathbf{x})$ of the weak derivative $f_u^{[1]}(\mathbf{x})$ of the prediction model $f_u(\mathbf{x})$ is obtained element-wise as: for $r^{\dagger} \in \{2, 3, \dots, R\}, k^{\dagger} \in [d], \ell^{\dagger} \in [L]$ and $u \in \mathcal{U}$, we have

$$\frac{\partial}{\partial \phi} f_u^{[1]}(\mathbf{x}_i) = 0,$$

$$\begin{aligned}
\frac{\partial}{\partial \varphi_{r^\dagger}} f_u^{[1]}(\mathbf{x}_i) &= \mathbb{1}(u \in \mathcal{U}_{r^\dagger-1}) \frac{\text{sign}(\varphi_{r^\dagger})}{j_{r^\dagger} - j_{r^\dagger-1}}, \\
\frac{\partial}{\partial v_{k^\dagger, \ell^\dagger}^{(1)}} f_u^{[1]}(\mathbf{x}_i) &= x_{ik^\dagger} \frac{\partial}{\partial v_{k^\dagger, \ell^\dagger}^{(1)}} b_{k^\dagger}^{[1]}(u) = x_{ik^\dagger} w_{k^\dagger, \ell^\dagger}^{(2)} w_{k^\dagger, \ell^\dagger}^{(1)} \rho^{[2]}(w_{k^\dagger, \ell^\dagger}^{(1)} u + v_{k^\dagger, \ell^\dagger}^{(1)}), \\
\frac{\partial}{\partial v_{k^\dagger}^{(2)}} f_u^{[1]}(\mathbf{x}_i) &= x_{ik^\dagger} \frac{\partial}{\partial v_{k^\dagger}^{(2)}} b_{k^\dagger}^{[1]}(u) = 0, \\
\frac{\partial}{\partial w_{k^\dagger, \ell^\dagger}^{(1)}} f_u^{[1]}(\mathbf{x}_i) &= x_{ik^\dagger} \frac{\partial}{\partial w_{k^\dagger, \ell^\dagger}^{(1)}} b_{k^\dagger}^{[1]}(u) = x_{ik^\dagger} w_{k^\dagger, \ell^\dagger}^{(2)} w_{k^\dagger, \ell^\dagger}^{(1)} u \rho^{[2]}(w_{k^\dagger, \ell^\dagger}^{(1)} u + v_{k^\dagger, \ell^\dagger}^{(1)}) \\
&\quad + x_{ik^\dagger} w_{k^\dagger, \ell^\dagger}^{(2)} \rho^{[1]}(w_{k^\dagger, \ell^\dagger}^{(1)} u + v_{k^\dagger, \ell^\dagger}^{(1)}), \\
\frac{\partial}{\partial w_{k^\dagger, \ell^\dagger}^{(2)}} f_u^{[1]}(\mathbf{x}_i) &= x_{ik^\dagger} \frac{\partial}{\partial w_{k^\dagger, \ell^\dagger}^{(2)}} b_{k^\dagger}^{[1]}(u) = x_{ik^\dagger} w_{k^\dagger, \ell^\dagger}^{(1)} \rho^{[1]}(w_{k^\dagger, \ell^\dagger}^{(1)} u + v_{k^\dagger, \ell^\dagger}^{(1)}).
\end{aligned}$$

A.3 Gradient of the log-likelihood

Using the conditional probability density function (6), we have

$$\begin{aligned}
\nabla_{\boldsymbol{\theta}} \ell_{\boldsymbol{\zeta}}(\boldsymbol{\theta}) &= \sum_{i=1}^n \zeta_i \nabla_{\boldsymbol{\theta}} \log q(h_i | \mathbf{x}_i) \\
&= \sum_{i=1}^n \zeta_i \nabla_{\boldsymbol{\theta}} \{\log \sigma^{[1]}(f_{h_i}(\mathbf{x}_i)) + \log f_{h_i}^{[1]}(\mathbf{x}_i)\} \\
&= \sum_{i=1}^n \zeta_i \left\{ \frac{\sigma^{[2]}(f_{h_i}(\mathbf{x}_i))}{\sigma^{[1]}(f_{h_i}(\mathbf{x}_i))} \nabla_{\boldsymbol{\theta}} f_{h_i}(\mathbf{x}_i) + \frac{1}{f_{h_i}^{[1]}(\mathbf{x}_i)} \nabla_{\boldsymbol{\theta}} f_{h_i}^{[1]}(\mathbf{x}_i) \right\}.
\end{aligned}$$

Together with the gradient of f_u and $f_u^{[1]}$, gradient of the log-likelihood is obtained element-wise as follows. For $r^\dagger \in \{2, 3, \dots, R\}$, $k^\dagger \in [d]$, $\ell^\dagger \in [L]$, we have

$$\begin{aligned}
\frac{\partial}{\partial \phi} \ell_{\boldsymbol{\zeta}}(\boldsymbol{\theta}) &= \sum_{i=1}^n \zeta_i \frac{\sigma^{[2]}(f_{h_i}(\mathbf{x}_i))}{\sigma^{[1]}(f_{h_i}(\mathbf{x}_i))}, \\
\frac{\partial}{\partial \varphi_{r^\dagger}} \ell_{\boldsymbol{\zeta}}(\boldsymbol{\theta}) &= \text{sign}(\varphi_{r^\dagger}) \sum_{i=1}^n \zeta_i \frac{\sigma^{[2]}(f_{h_i}(\mathbf{x}_i))}{\sigma^{[1]}(f_{h_i}(\mathbf{x}_i))} \left\| \frac{h_i - j_{r^\dagger-1}}{j_{r^\dagger} - j_{r^\dagger-1}} \right\| \\
&\quad + \frac{\text{sign}(\varphi_{r^\dagger})}{j_{r^\dagger} - j_{r^\dagger-1}} \sum_{i=1}^n \zeta_i \mathbb{1}(h_i \in \mathcal{U}_{r^\dagger-1}) \frac{1}{f_{h_i}^{[1]}(\mathbf{x}_i)}, \\
\frac{\partial}{\partial v_{k^\dagger, \ell^\dagger}^{(1)}} \ell_{\boldsymbol{\zeta}}(\boldsymbol{\theta}) &= \sum_{i=1}^n \zeta_i \frac{\sigma^{[2]}(f_{h_i}(\mathbf{x}_i))}{\sigma^{[1]}(f_{h_i}(\mathbf{x}_i))} x_{ik^\dagger} w_{k^\dagger, \ell^\dagger}^{(2)} w_{k^\dagger, \ell^\dagger}^{(1)} \rho^{[1]}(w_{k^\dagger, \ell^\dagger}^{(1)} h_i + v_{k^\dagger, \ell^\dagger}^{(1)}) \\
&\quad + \sum_{i=1}^n \zeta_i \frac{1}{f_{h_i}^{[1]}(\mathbf{x}_i)} x_{ik^\dagger} w_{k^\dagger, \ell^\dagger}^{(2)} w_{k^\dagger, \ell^\dagger}^{(1)} \rho^{[2]}(w_{k^\dagger, \ell^\dagger}^{(1)} h_i + v_{k^\dagger, \ell^\dagger}^{(1)}), \\
\frac{\partial}{\partial v_{k^\dagger}^{(2)}} \ell_{\boldsymbol{\zeta}}(\boldsymbol{\theta}) &= \sum_{i=1}^n \zeta_i \frac{\sigma^{[2]}(f_{h_i}(\mathbf{x}_i))}{\sigma^{[1]}(f_{h_i}(\mathbf{x}_i))} x_{ik^\dagger}, \\
\frac{\partial}{\partial w_{k^\dagger, \ell^\dagger}^{(1)}} \ell_{\boldsymbol{\zeta}}(\boldsymbol{\theta}) &= \sum_{i=1}^n \zeta_i \frac{\sigma^{[2]}(f_{h_i}(\mathbf{x}_i))}{\sigma^{[1]}(f_{h_i}(\mathbf{x}_i))} x_{ik^\dagger} w_{k^\dagger, \ell^\dagger}^{(2)} h_i \rho^{[1]}(w_{k^\dagger, \ell^\dagger}^{(1)} h_i + v_{k^\dagger, \ell^\dagger}^{(1)}) \\
&\quad + \sum_{i=1}^n \zeta_i \frac{1}{f_{h_i}^{[1]}(\mathbf{x}_i)} \left\{ x_{ik^\dagger} w_{k^\dagger, \ell^\dagger}^{(2)} w_{k^\dagger, \ell^\dagger}^{(1)} h_i \rho^{[2]}(w_{k^\dagger, \ell^\dagger}^{(1)} h_i + v_{k^\dagger, \ell^\dagger}^{(1)}) \right.
\end{aligned}$$

$$\begin{aligned}
& + x_{ik^\dagger} w_{k^\dagger, \ell^\dagger}^{(2)} \rho^{[1]}(w_{k^\dagger, \ell^\dagger}^{(1)} h_i + v_{k^\dagger, \ell^\dagger}^{(1)}) \}, \\
\frac{\partial}{\partial w_{k^\dagger, \ell^\dagger}^{(2)}} \ell \zeta(\boldsymbol{\theta}) &= \sum_{i=1}^n \zeta_i \frac{\sigma^{[2]}(f_{h_i}(\mathbf{x}_i))}{\sigma^{[1]}(f_{h_i}(\mathbf{x}_i))} x_{ik^\dagger} \rho(w_{k^\dagger, \ell^\dagger}^{(1)} h_i + v_{k^\dagger, \ell^\dagger}^{(1)}) \\
& + \sum_{i=1}^n \zeta_i \frac{1}{f_{h_i}^{[1]}(\mathbf{x}_i)} x_{ik^\dagger} w_{k^\dagger, \ell^\dagger}^{(1)} \rho^{[1]}(w_{k^\dagger, \ell^\dagger}^{(1)} h_i + v_{k^\dagger, \ell^\dagger}^{(1)}).
\end{aligned}$$

B Initialization

With given parameter vectors $\hat{\boldsymbol{\beta}}_j = (\hat{\beta}_{j1}, \hat{\beta}_{j2}, \dots, \hat{\beta}_{jd})^\top$ ($j = 1, 2, \dots, J$), that are preliminarily computed by existing algorithm for (discrete) NPOM, we initialize the neural network parameters so as to satisfy

$$b_k(j) \approx \hat{\beta}_{jk}, \quad (j = 1, 2, \dots, J; k = 1, 2, \dots, d). \quad (17)$$

In our implementation, we employ the vectors $\hat{\boldsymbol{\beta}}_1, \hat{\boldsymbol{\beta}}_2, \dots, \hat{\boldsymbol{\beta}}_{J-1}$ computed by `serp` package in R language, and specify $\hat{\boldsymbol{\beta}}_J = \hat{\boldsymbol{\beta}}_{J-1} + (\hat{\boldsymbol{\beta}}_{J-1} - \hat{\boldsymbol{\beta}}_{J-2}) = 2\hat{\boldsymbol{\beta}}_{J-1} - \hat{\boldsymbol{\beta}}_{J-2}$ formally.

To satisfy the equality (17), we employ a NN using sigmoid activation function $\rho(z) = 1/(1 + \exp(-z))$ and $L > d$; with a sufficiently large constant T (e.g., $T = 10$, satisfying $\rho(-T) \approx 0, \rho(+T) \approx 1$), we define

$$\begin{aligned}
v_k^{(2)} &= \frac{1}{J} \sum_{j=1}^J \hat{\beta}_{jk}, \\
v_{k, \ell}^{(1)} &= \begin{cases} -T\ell & (\ell \in \{1, 2, \dots, J\}) \\ 0 & (\text{Otherwise}) \end{cases}, \\
w_{k, \ell}^{(1)} &= \begin{cases} T & (\ell \in \{1, 2, \dots, J\}) \\ 0 & (\text{Otherwise}) \end{cases}, \\
w_{k, \ell}^{(2)} &= \begin{cases} \frac{\hat{\beta}_{\ell k} - v_k^{(2)} - \sum_{\ell'=1}^{\ell-1} w_{k, \ell'}^{(2)}}{\rho(0)} & (\ell \in \{1, 2, \dots, J\}) \\ 0 & (\text{Otherwise}) \end{cases},
\end{aligned}$$

for all $k \in \{1, 2, \dots, d\}$. Then, we have

$$\begin{aligned}
b_k(j) &= \sum_{\ell=1}^L w_{k, \ell}^{(2)} \rho(w_{k, \ell}^{(1)} j + v_{k, \ell}^{(1)}) + v_k^{(2)} \\
&= \sum_{\ell=1}^J w_{k, \ell}^{(2)} \rho(T(j - \ell)) + v_k^{(2)} \\
&\approx \sum_{\ell=1}^J w_{k, \ell}^{(2)} \{\rho(-\infty) \mathbb{1}(j < \ell) + \rho(0) \mathbb{1}(\ell = j) + \rho(\infty) \mathbb{1}(\ell < j)\} + v_k^{(2)} \\
&= w_{k, j}^{(2)} \rho(0) + \sum_{\ell=1}^{j-1} w_{k, \ell}^{(2)} + v_k^{(2)} \\
&= \frac{\hat{\beta}_{jk} - v_k^{(2)} - \sum_{\ell=1}^{j-1} w_{k, \ell}^{(2)}}{\rho(0)} \rho(0) + \sum_{\ell=1}^{j-1} w_{k, \ell}^{(2)} + v_k^{(2)} \\
&= \hat{\beta}_{jk}.
\end{aligned}$$

For more stability of the NN training, in our implementation, the non-zero weights in $\{w_{k, \ell}^{(2)}\}$ divided by $T = \max_{t \in \mathbb{N}} \{L/J \geq t\}$ are duplicated T times, and the non-zero weights in $\{w_{k, \ell}^{(1)}\}, \{v_{k, \ell}^{(1)}\}$ are also duplicated T times. I.i.d. standard normal random numbers are added to the remaining zero-weights. By this duplication, the weights distribute more uniformly compared to the setting that only a few non-zero weights exist, so the subsequent neural network training is expected to be more stable.

C Proofs

Proof of Proposition 1. We employ a proof by contradiction. As \mathcal{U} is a compact set, $s := \text{esssup}_{u \in [1, J]} a^{[1]}(u) > 0$ holds. Suppose there exists $(u', \mathbf{x}') \in \mathcal{U} \times \mathbb{R}^d$ such that $|\nabla_u \langle \mathbf{b}(u'), \mathbf{x}' \rangle| > 0$. Then, we may assume $t_{u', \mathbf{x}'} := \nabla_u \langle \mathbf{b}(u'), \mathbf{x}' \rangle > 0$ without loss of generality (consider $-\mathbf{x}'$ insted if $\nabla_u \langle \mathbf{b}(u'), \mathbf{x}' \rangle < 0$). Then, by taking $L := (s/t_{u', \mathbf{x}'}) + 1$, we have

$$\nabla_u f_{u'}(-L\mathbf{x}') < s - L\nabla_u \langle \mathbf{b}(u'), \mathbf{x}' \rangle < s - (\{s/t_{u', \mathbf{x}'}\} + 1)t_{u', \mathbf{x}'} = -t_{u', \mathbf{x}'} < 0$$

almost surely. At the point $-L\mathbf{x}'$, $f_u(-L\mathbf{x})$ is decreasing with respect to u , over a sufficiently small open ball around u' ; contradiction is derived. Thus $|\nabla_u \langle \mathbf{b}(u), \mathbf{x} \rangle| = 0$ holds for all $(u, \mathbf{x}) \in \mathcal{U} \times \mathbb{R}^d$. Together with the continuity of the function \mathbf{b} , $\mathbf{b}(u)$ is a constant function. \square

Proof of Proposition 2. As the weak derivative is obtained as

$$\langle \mathbf{b}^{[1]}(u), \mathbf{x} \rangle = \sum_{k=1}^d x_k b_k^{[1]}(u) = \sum_{k=1}^d x_k \sum_{\ell=1}^L w_{k, \ell}^{(2)} w_{k, \ell}^{(1)} \rho^{[1]}(w_{k, \ell}^{(1)} u + v_{k, \ell}^{(1)}),$$

Cauchy-Schwarz inequality proves an inequality

$$\begin{aligned} |\langle \mathbf{b}^{[1]}(u), \mathbf{x} \rangle| &\leq \sqrt{\sum_{k=1}^d x_k^2} \sqrt{\sum_{k=1}^d \left\{ \sum_{\ell=1}^L w_{k, \ell}^{(2)} w_{k, \ell}^{(1)} \rho^{[1]}(w_{k, \ell}^{(1)} u + v_{k, \ell}^{(1)}) \right\}^2} \\ &< \eta \cdot \rho_\infty^{[1]} \cdot \sqrt{\sum_{k=1}^d \left\{ \sum_{\ell=1}^L |w_{k, \ell}^{(2)} w_{k, \ell}^{(1)}| \right\}^2} \end{aligned} \quad (18)$$

for $\mathbf{x} = (x_1, x_2, \dots, x_d) \in \mathcal{X}_2(\eta)$. This inequality indicates that

$$f_u^{[1]}(\mathbf{x}) = a^{[1]}(u) + \langle \mathbf{b}^{[1]}(u), \mathbf{x} \rangle \stackrel{(18)}{\geq} \min_{r=2,3,\dots,R-1} s_{r-1} - \eta \cdot \rho_\infty^{[1]} \cdot \sqrt{\sum_{k=1}^d \left\{ \sum_{\ell=1}^L |w_{k, \ell}^{(2)} w_{k, \ell}^{(1)}| \right\}^2} \stackrel{(13)}{\geq} 0,$$

where the non-negativity of the right-most side is obtained by the inequality (13). As $f_u^{[1]}$ is a weak derivative of the function f_u , f_u is non-decreasing. As the above calculation holds for all \mathbf{x} , the continuity of f_u proves the assertion. \square

References

- Agresti, A. (2010). *Analysis of Ordinal Categorical Data*. John Wiley & Sons.
- Bennett, S. (1983). Log-logistic regression models for survival data. *Journal of the Royal Statistical Society. Series C (Applied Statistics)*, 32(2):165–171.
- Cybenko, G. (1989). Approximation by superpositions of a sigmoidal function. *Mathematics of Control, Signals and Systems*, 2(4):303–314.
- Dua, D. and Graff, C. (2017). UCI machine learning repository.
- Goodfellow, I., Bengio, Y., and Courville, A. (2016). *Deep Learning*. MIT Press. <http://www.deeplearningbook.org>.
- Hastie, T. and Tibshirani, R. (1993). Varying-coefficient models. *Journal of the Royal Statistical Society. Series B (Methodological)*, 55(4):757–796.

- Kalbfleisch, J. D. and Prentice, R. L. (2002). *The Statistical Analysis of Failure Time Data*. John Wiley & Sons, Inc., 2nd edition.
- Liu, Q., Shepherd, B. E., Li, C., and Harrell, Jr, F. E. (2017). Modeling continuous response variables using ordinal regression. *Statistics in Medicine*, 36(27):4316–4335.
- Long, J. S. and Freese, J. (2006). *Regression models for categorical dependent variables using Stata*, volume 7. Stata press.
- Lu, F., Ferraro, F., and Raff, E. (2022). Continuously generalized ordinal regression for linear and deep models. In *Proceedings of the 2022 SIAM International Conference on Data Mining (SDM)*, pages 28–36. SIAM.
- McCullagh, P. (1980). Regression models for ordinal data. *Journal of Royal Statistical Society. Series B (Methodological)*, 42(2):109–127.
- McCullagh, P. and Nelder, J. A. (1989). *Generalized Linear Models*. Chapman & Hall CRC, London.
- Peterson, B. and Harrell, F. E. (1990). Partial proportional odds models for ordinal response variables. *Journal of Royal Statistical Society. Series C (Applied Statistics)*, 39(2):205–217.
- Satoh, K., Tonda, T., and Izumi, S. (2016). Logistic regression model for survival time analysis using time-varying coefficients. *American Journal of Mathematical and Management Sciences*, 35(4):353–360.
- Thas, O., Neve, J. D., Clement, L., and Ottoy, J.-P. (2012). Probabilistic index models. *Journal of Royal Statistical Society. Series B (Methodological)*, 74(4):623–671.
- Tutz, G. and Berger, M. (2022). Sparser ordinal regression models based on parametric and additive location-shift approaches. *International Statistical Review*, 90(2):306–327.
- Tutz, G. and Gertheiss, J. (2016). Regularized regression for categorical data. *Statistical Modelling*, 16(3):161–200.
- Ugba, E. R., Mörlein, D., and Gertheiss, J. (2021). Smoothing in ordinal regression: An application to sensory data. *Stats*, 4(3):616–633.
- Williams, R. (2006). Generalized ordered logit/partial proportional odds models for ordinal dependent variables. *Stata Journal*, 6:58–82.
- Williams, R. (2016). Understanding and interpreting generalized ordered logit models. *The Journal of Mathematical Sociology*, 40(1):7–20.
- Wurm, M. J., Rathouz, P. J., and Hanlon, B. M. (2021). Regularized ordinal regression and the ordinalNet R package. *Journal of Statistical Software*, 99(6).

Supplementary material:

“An interpretable neural network-based non-proportional odds model for ordinal regression”.

A. Okuno (*okuno@ism.ac.jp*) and K. Harada (*haradak@tokyo-med.ac.jp*).

D Additional experiments.

In addition to the autoMPG6, autoMPG8, and real-estate datasets used in the main body of the paper, we collected boston-housing, concrete, and airfoil datasets from UCI machine learning repository (Dua and Graff, 2017). We train the N^3 POM by leveraging these datasets described in the following, and their results are shown in Figures 6–8.

The existing `serp` function used for initializing N^3 POM is time-consuming for larger datasets. Therefore, for the datasets with $n > 2000$, we first choose 2000 samples uniformly randomly, and apply `serp` function to the selected samples for initialization. Subsequently, we apply MPS algorithm to train N^3 POM using the entire dataset.

boston-housing ($n = 506, d = 12$). boston-housing dataset consists of 12 covariates (“`crim`” (continuous), “`zn`” (continuous), “`indus`” (continuous), “`chas`” (binary), “`nox`” (continuous), “`rm`” (continuous), “`age`” (continuous), “`dis`” (continuous), “`rad`” (discrete), “`tax`” (continuous), “`ptratio`” (continuous), “`lstat`” (continuous)) and a continuous response (“`medv`”) representing the housing price in boston. We preliminarily removed the “black” row for fairness. Descriptions of the covariates are provided in the caption of Figure 6.

concrete ($n = 1030, d = 8$). concrete dataset consists of 8 covariates (“`Cement`” (continuous), “`BlastFurnaceSlag`” (continuous), “`FlyAsh`” (continuous), “`Water`” (continuous), “`Superplasticizer`” (continuous), “`CoarseAggregate`” (continuous), “`FineAggregate`” (continuous), “`Age`”(continuous)) and a continuous response (“`ConcreteCompressiveStrength`”).

airfoil ($n = 1503, d = 5$). airfoil dataset consists of 5 covariates (frequency in hertz “`freq`” (continuous), angle of attack in degrees “`angle`” (continuous), chord length in meters “`chord`” (continuous), free-stream velocity in meters “`velocity`” (continuous), suction side displacement thickness in meters “`disp. thickness`” (continuous) and a continuous response “`sound pressure`” representing the scaled sound pressure level in decibels.

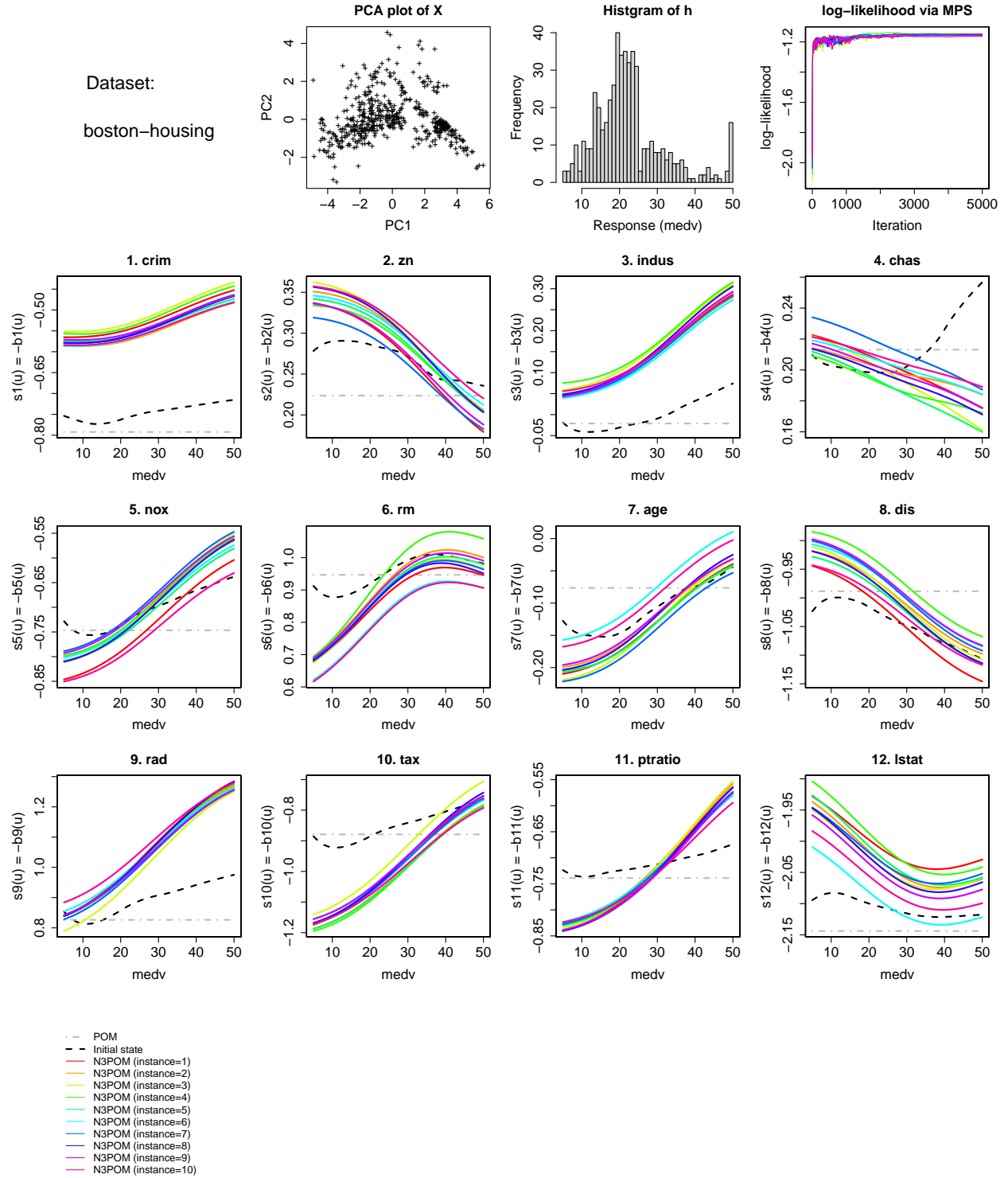


Figure 6: Boston-housing dataset experiment.

(**Covariates**) **crim**: per capita crime rate by town, **zn**: proportion of residential land zoned for lots over 25,000 sq.ft, **indus**: proportion of non-retail business acres per town, **chas**: Charles River dummy variable (=1 the house is located next to the river; 0 otherwise), **nox**: nitric oxides concentration (parts per 10 million), **rm**: average number of rooms per dwelling, **age**: proportion of owner-occupied units built prior to 1940, **dis**: weighted distances to five Boston employment centres, **rad**: index of accessibility to radial highways, **tax**: full-value property-tax rate per \$10,000, **ptratio**: pupil-teacher ratio by town, **lstat**: lower status of the population.

(**Response**) **medv**: Median value of owner-occupied homes in \$1000's.

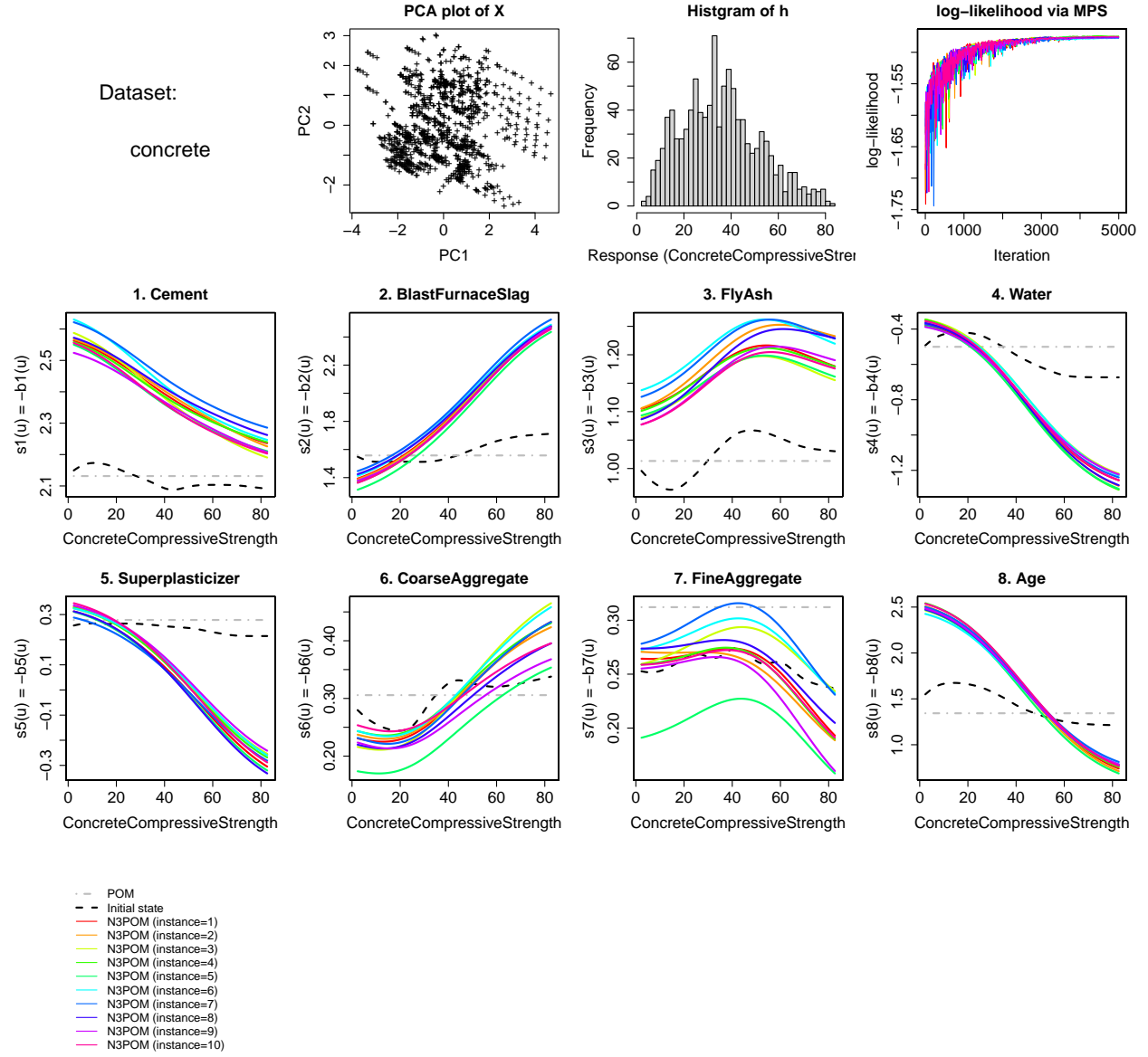


Figure 7: concrete dataset experiment.

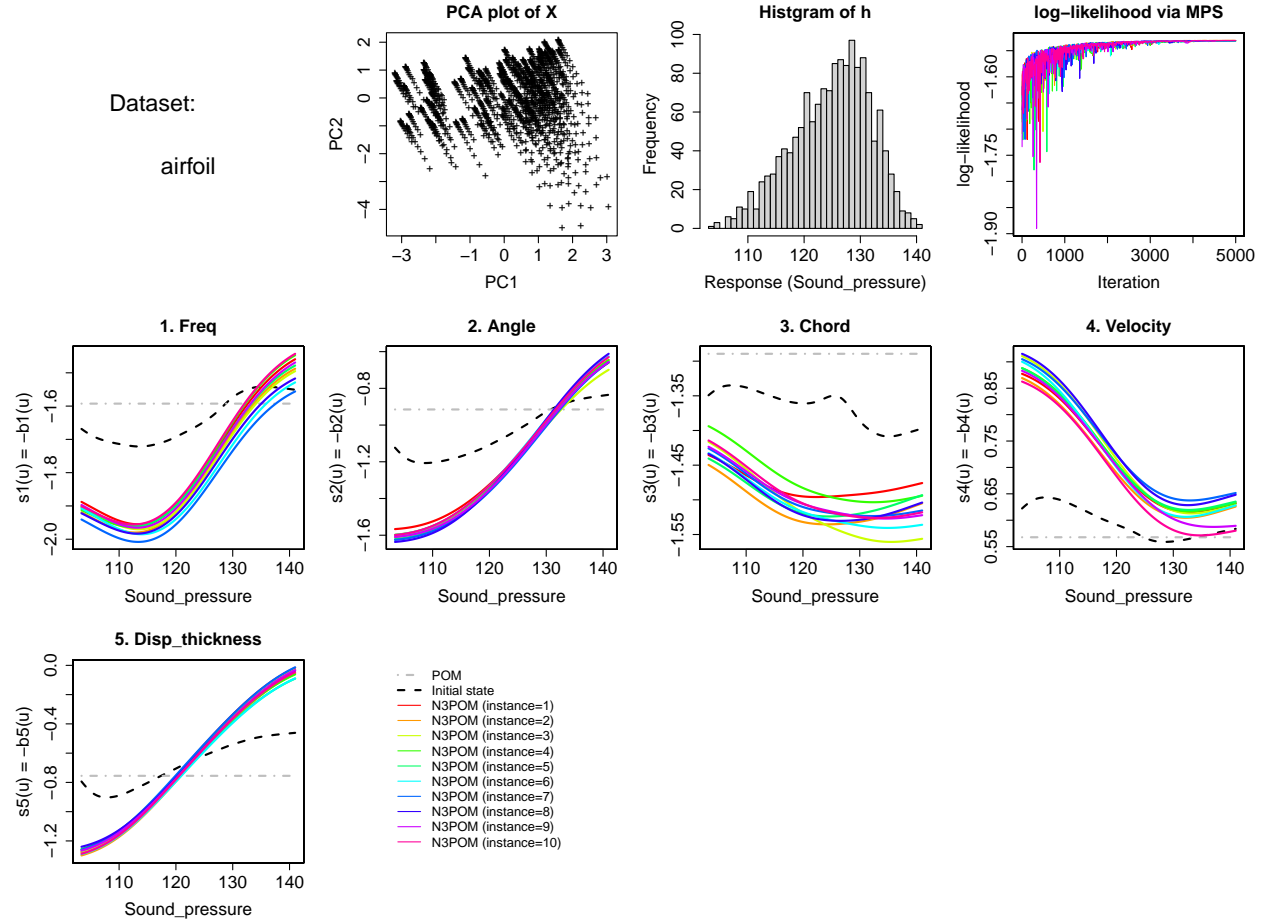


Figure 8: airfoil dataset experiment.

E Summary of datasets.

Covariates and response in autoMPG8, real-estate, boston-housing, concrete, airfoil, and cycle power-plant datasets are summarized in Figures 9–13. These plots are generated by `pairs.panels` function in `psych` package¹. Therein, the scatter plots for each pair of covariates, and their correlation coefficients are provided. We omit the plot for autoMPG6 as it is completely subsumed in autoMPG8. Note that the covariates and responses are preliminarily standardized by following the procedure described in Section 5.1.

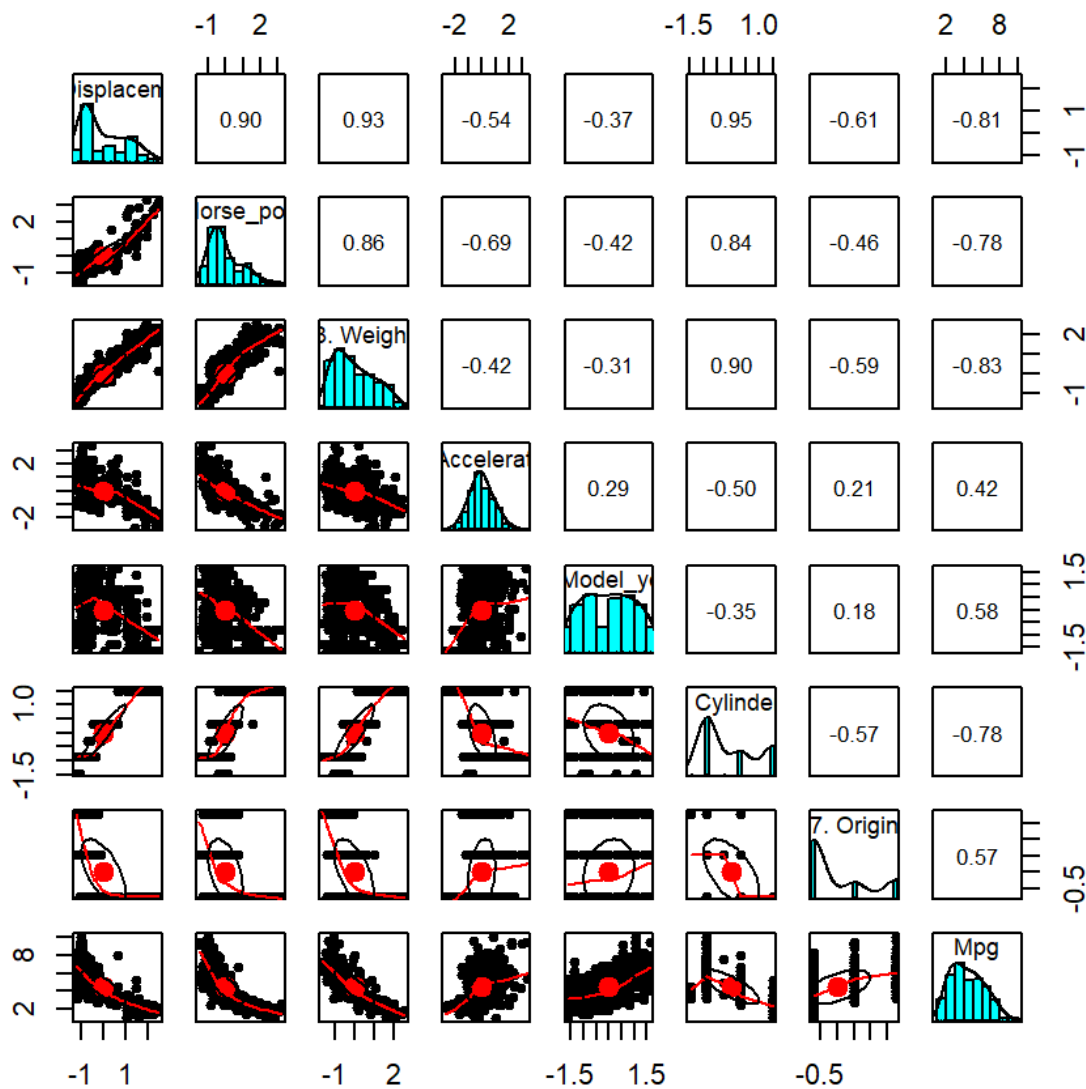


Figure 9: Summary of autoMPG8 dataset (subsuming autoMPG6 dataset).

¹<https://cran.r-project.org/package=psych>

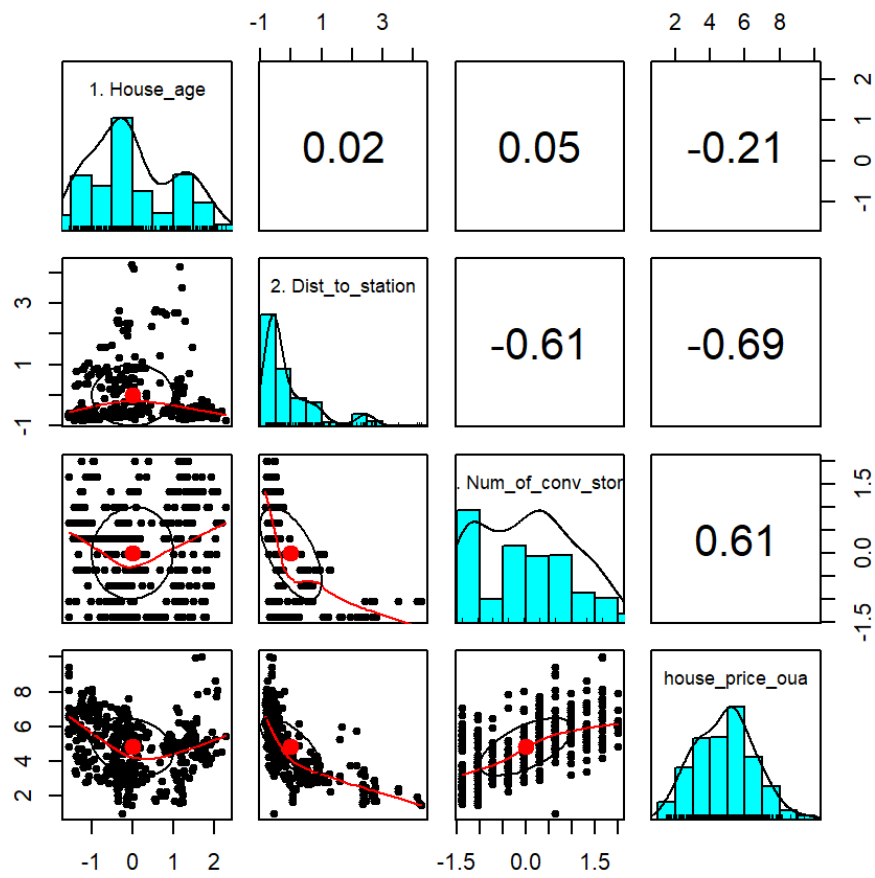


Figure 10: Summary of real-estate dataset.

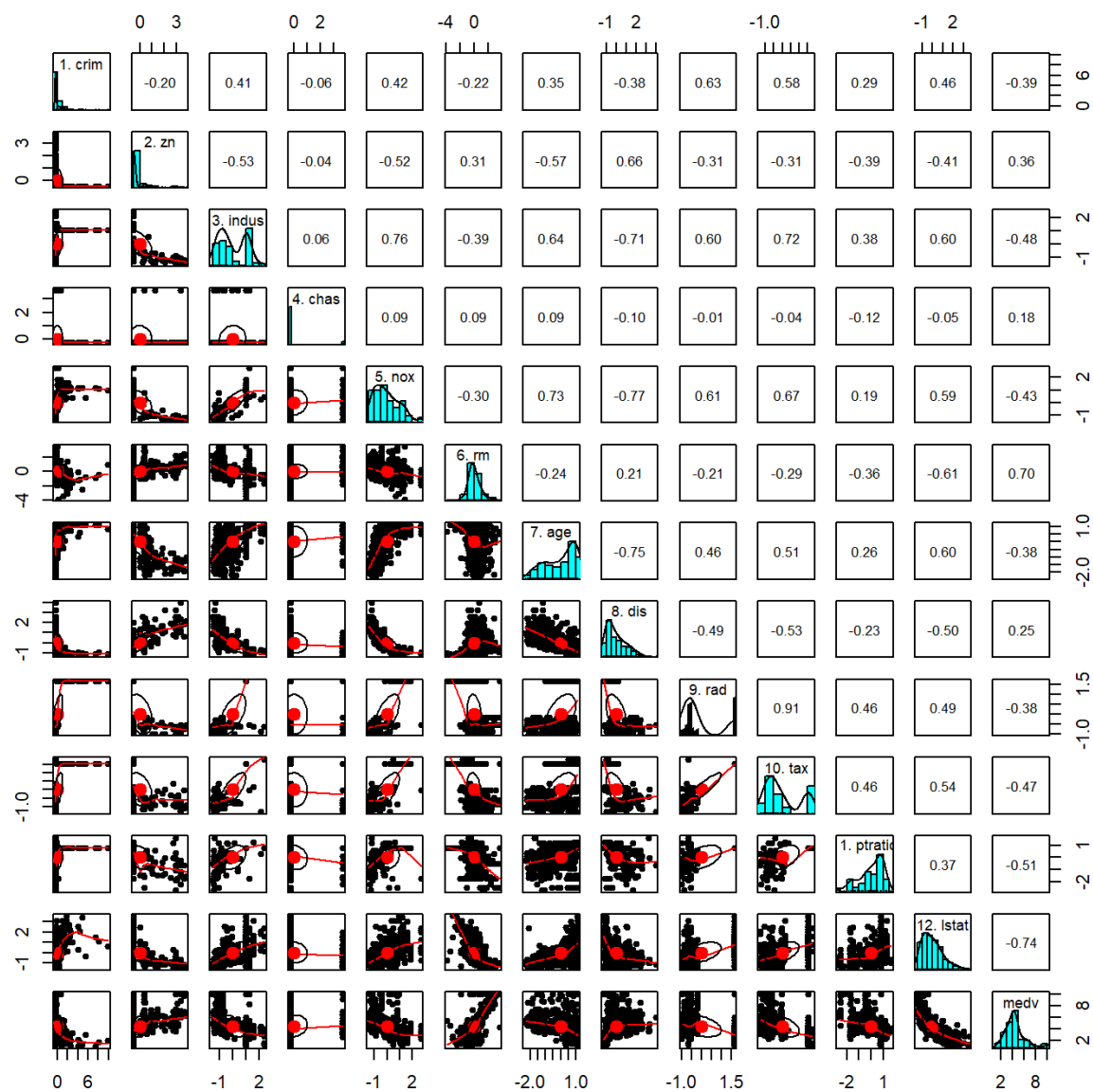


Figure 11: Summary of boston-housing dataset.

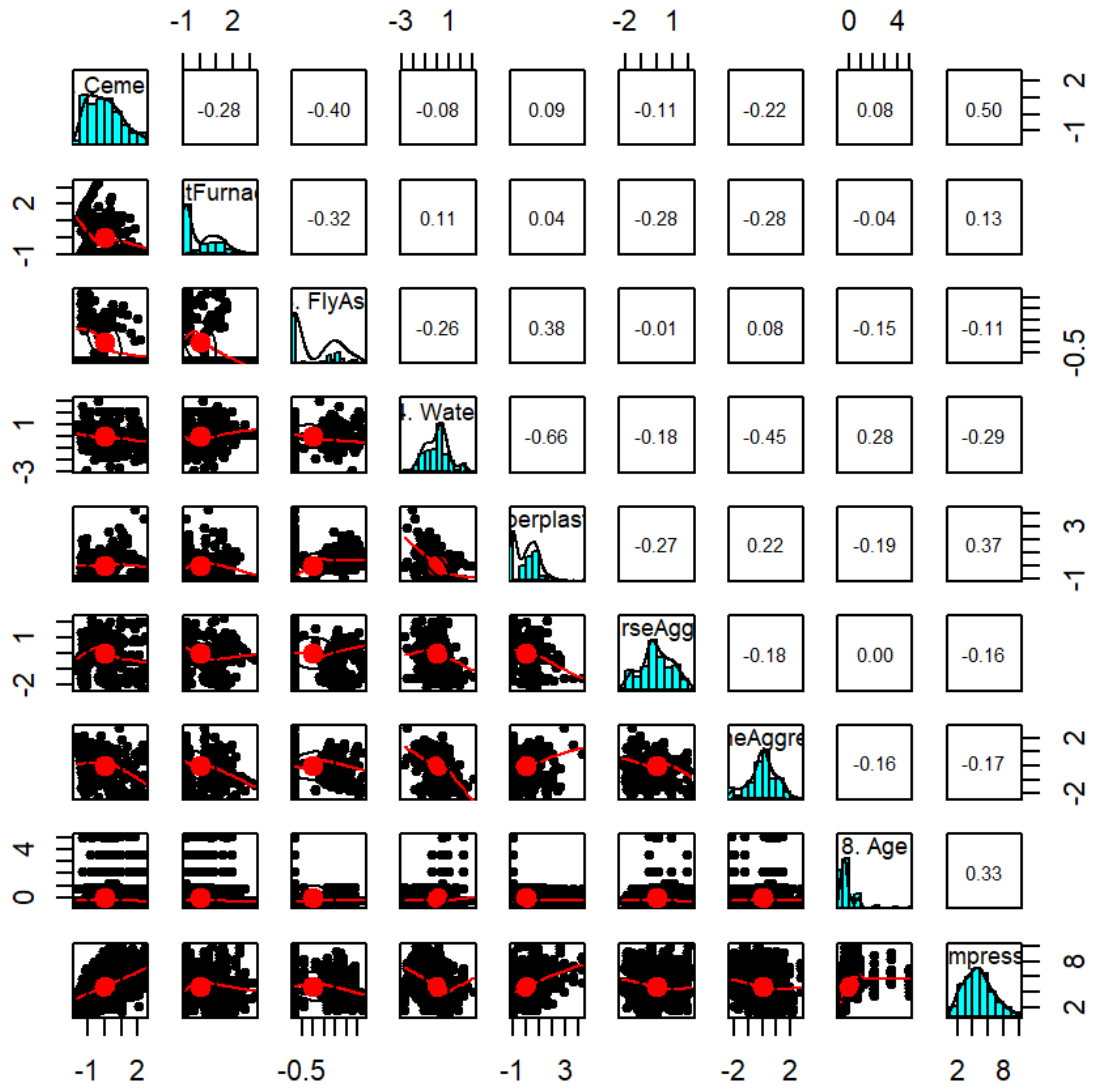


Figure 12: Summary of concrete dataset.

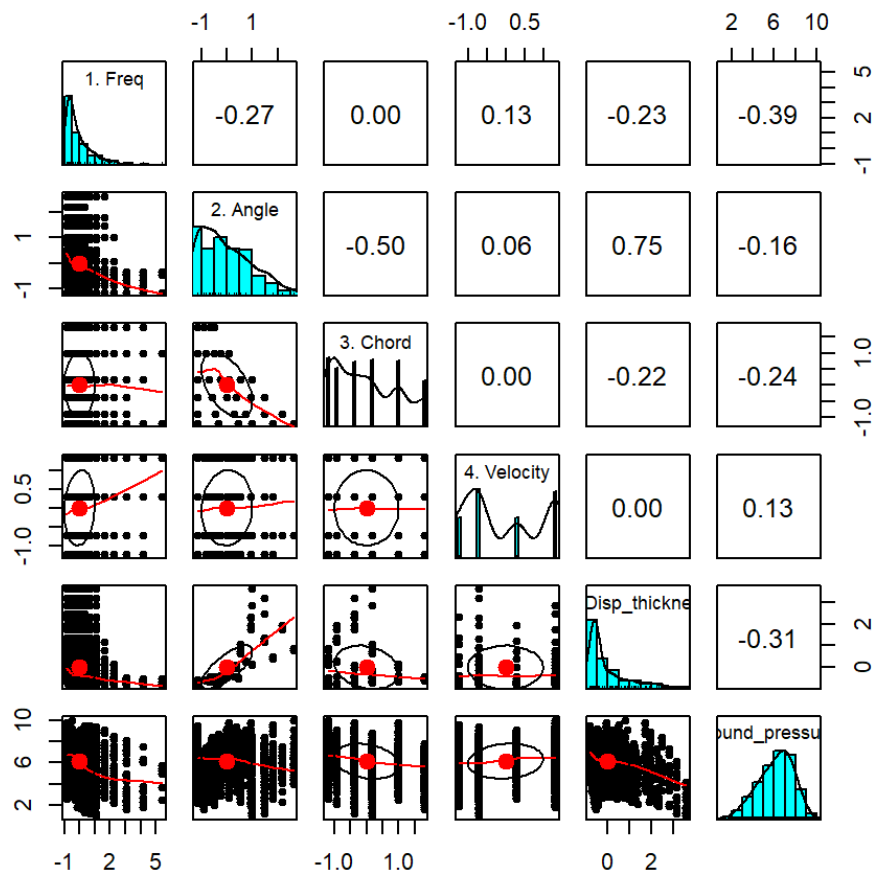


Figure 13: Summary of airfoil dataset.